PLANT SCIENCES

A plant peptide with dual activity against multidrug-resistant bacterial and fungal pathogens

Xueyan Chen[1]†, Meirong Song[2]†, Lei Tian[1]†, Xinxin Shan[3], Changsi Mao[2], Minghui Chen[1], Jiaqi Zhao[1], Abdul Sami[1], Haoqiang Yin[1], Usman Ali[1], Jiawei Shi[1], Hehuan Li[1], Yuqian Zhang[1], Jinghua Zhang[1], Shunxi Wang[1], Chun-Lin Shi[1], Yanhui Chen[1], Xiang-Dang Du[3]*, Kui Zhu[2]*, Liuji Wu[1]*

Multidrug-resistant (MDR) bacteria pose a major threat to public health, and additional sources of antibacterial candidates are urgently needed. Noncanonical peptides (NCPs), derived from noncanonical small open reading frames, represent small biological molecules with important roles in biology. However, the antibacterial activity of NCPs remains largely unknown. Here, we discovered a plant-derived noncanonical antibacterial peptide (NCBP1) against both Gram-positive and Gram-negative bacteria. NCBP1 is composed of 11 amino acid residues with cationic surface potential and favorable safety and stability. Mechanistic studies revealed that NCBP1 displayed antibacterial activity by targeting phosphatidylglycerol and cardiolipin in bacterial membrane, resulting in membrane damage and dysfunction. Notably, NCBP1 showed promising efficacy in mice. Furthermore, NCBP1 effectively inhibited the growth of plant fungal pathogens and enhanced disease resistance in maize. Our results demonstrate the unexplored antimicrobial potential of plant-derived NCPs and provide an accessible source for the discovery of antimicrobial substances against MDR bacterial and fungal pathogens.

INTRODUCTION

Pathogenic bacteria cause severe illness and notable mortality globally (*1*). The discovery of antibiotics and their subsequent introduction into the clinic have saved countless individuals suffering from bacterial infections (*2*). However, the indiscriminate misuse and overuse of antibiotics have ultimately reduced their efficacy and driven the emergence and dissemination of multidrug-resistant (MDR) bacteria (*3*–*5*). Such pathogens are increasingly overwhelming for nosocomial treatments worldwide (*6*, *7*), leaving clinicians with few or no choices from the current antibiotic pipelines. Therefore, there is an urgent need for discovery of alternative antibacterial agents to combat MDR infections.

Peptides are chains linked by amide bonds of 2 to 100 amino acid residues and are well known as small biological molecules with important functional roles (*8*). Over the last few decades, antibacterial peptides (ABPs) with pronounced activities have been described (*9*–*14*). ABPs mainly include canonical peptides (CPs) derived from canonical open reading frames (ORFs) (*10*, *15*), such as LL-37 (*16*), and nonribosomal peptides biosynthesized through nonribosomal synthesis pathways (*17*), such as colistin (*18*) (Fig. 1A). However, MDR bacteria have evolved diverse resistance mechanisms against these conventional ABPs (*15*, *19*–*21*). Recently, an emerging class of peptides, noncanonical peptides (NCPs), derived from noncanonical small ORFs, such as intergenic regions, 5′ untranslated regions (UTRs), 3′UTRs, intronic regions, and various types of junctions, has attracted great attention (*22*). Previous studies have demonstrated that NCPs play essential roles in various physiological and biological processes (*23*, *24*). For instance, Aw112010, an NCP derived from animal macrophages, displays antibacterial activity against *Salmonella* Typhimurium (*25*), indicating that NCP is an emerging resource for discovering alternative antibacterial agents against bacterial infections. However, the antibacterial potential of plant-derived NCPs has yet to be reported (Fig. 1A).

Plants generate a wide variety of natural products that have evolved for a particular biological function, serving as a reservoir for drug discovery in the field of infection treatment (*21*, *26*, *27*). Maize (*Zea mays* L.), one of the most important crop plants globally, is a keystone model organism as well. On the basis of our homemade library of maize NCPs (*22*), herein we aimed to identify and evaluate the antibacterial potential of maize-derived NCPs using a large-scale screening approach. As a result, we identified a plant-derived noncanonical ABP, NCBP1. This candidate showed broad-spectrum antibacterial activities against both MDR Gram-positive and Gram-negative bacteria. Moreover, NCBP1 displayed a membrane-dependent mechanism by binding to phosphatidylglycerol (PG) and cardiolipin (CL). In addition, we demonstrated that NCBP1 showed efficient anti-infective activity against MDR bacteria in vivo. Given the considerable impact of fungal pathogens on crop yield and global food security, coupled with the limitations of current fungicidal strategies including the development of resistance and environmental concerns (*28*), there is an urgent need for alternative and naturally derived antifungal agents. Therefore, we further explored the role of NCBP1 in plant disease resistance. Our results demonstrated that NCBP1 significantly inhibits the growth of fungal pathogens and enhances maize resistance to fungal diseases upon exogenous application. Our study highlights the potential of plant-derived NCPs as a diversified repository for developing antibacterial agents to combat MDR infections and antifungal agents to mitigate fungal threats in plants.

RESULTS

Screening the antibacterial potential of NCPs derived from maize

A library with the capacity of 1000 maize endogenous peptides was first generated based on our previous study (*22*), consisting of 894

[1]State Key Laboratory of High-Efficiency Production of Wheat-Maize Double Cropping, Center for Crop Genome Engineering, College of Agronomy, Henan Agricultural University, Zhengzhou 450046, China. [2]National Key Laboratory of Veterinary Public Health and Safety, College of Veterinary Medicine, China Agricultural University, Beijing 100193, China. [3]College of Veterinary Medicine, Henan Agricultural University, Zhengzhou 450046, China.
*Corresponding author. Email: xddu@henau.edu.cn (X.-D.D.); zhuk@cau.edu.cn (K.Z.); wlj200120@163.com (L.W.)
†These authors contributed equally to this work.

from intergenic regions, 12 from 5′UTRs, 13 from 3′UTRs, 74 from introns, and 7 from junctions (fig. S1 and table S1). These NCPs are characterized by molecular weights ranging from 645 to 2890 Da and consist of 6 to 27 amino acids (table S1). We then assessed the antibacterial activity of these NCPs against a panel of MDR pathogens, including four Gram-positive bacteria, *Staphylococcus cohnii* L5 [*cfr*, *mecA*, and *aac(6′)-aph(2″)*], *Enterococcus faecium* E1077 (*ermA* and *tetM*), *Listeria monocytogenes* NH1 (*ermB*, *aphA3*, and *lsaE*), and *Streptococcus suis* SC181 (*ermB*, *mefA*, and *optrA*), and two Gram-negative bacteria, *Escherichia coli* MLS9F (*mcr-1* and bla_{NDM-9}) and *Klebsiella pneumoniae* B (bla_{SHV} and *oqxAB*) (table S2). These prevalent MDR pathogens pose a serious threat to public health around the world. Subsequently, both agar diffusion assays and broth microdilution methods were used to verify the antibacterial potential of the NCPs (fig. S1). Encouragingly, we identified one candidate, a noncanonical ABP (NCBP1) (fig. S2), which demonstrated broad-spectrum antibacterial activity against all strains tested. The inhibition zones of NCBP1 ranged from 3.12 to 11.39 mm (Fig. 1, B and C), and the minimum inhibitory concentrations (MICs) were between 16 and 128 μM (table S3). Notably, NCBP1 exhibited promising antibacterial activity against *S. cohnii* L5, with an MIC of 16 μM (table S3). To further evaluate the bacterial spectrum of NCBP1, we subsequently determined the activity of NCBP1 against a panel of *Staphylococcus* spp. strains from animals, including methicillin-resistant *S. aureus*, *S. chromogenes*, *S. equorum*, *S. intermedius*, *S. lentus*, *S. simulans*, and *S. squirrel* (table S4). NCBP1 showed antibacterial activity against these strains, with MIC ranging from 16 to 64 μM (table S4). These results indicate that NCBP1 is a broad-spectrum ABP. Altogether, these findings suggest the unexplored antibacterial potential of plant-derived NCPs and highlight their potential as a source of antibacterial agents against MDR pathogens.

To characterize NCBP1 in maize, we analyzed its genomic information and physiochemical properties. The result revealed that NCBP1 was derived from an intergenic region on chromosome 8 of the B73 genome, located at about 15.8 kb upstream of the nearest protein-coding gene (Fig. 1D). NCBP1 consists of 11 amino acid residues. The three-dimensional (3D) structure of NCBP1 was predicted by AlphaFold2. The electrostatic potential on the surface of the 3D structure revealed that NCBP1 was a cationic peptide, consistent with the presence of positively charged lysine residue at position 1 (Lys^1) and arginine at position 5 (Arg^5) (Fig. 1, E and F). In addition, phylogenetic analyses showed that NCBP1 was most closely related to a glycine-rich peptide (GRPSp) (Fig. 1G), a broad-spectrum ABP found in mud crab (*29*). However, NCBP1 and GRPSp (linear CP) displayed distinct 3D structures (Fig. 1F and fig. S3), suggesting that NCBP1 is a distinct type of plant-derived ABP. Nevertheless, further experimental validation is needed to confirm the structure of these peptides.

NCBP1 exhibited rapid bactericidal activities

To better assess the potency of NCBP1, the antibacterial activity was first evaluated using *S. cohnii* L5, an MDR pathogen (table S5), which is widely associated with severe nosocomial infections (*30*). Compared to vancomycin, NCBP1 showed comparable efficacy and inhibited bacterial growth in a dose-dependent manner (Fig. 2A), based on the analysis of growth curves. We then implemented time-killing kinetics of NCBP1 to further investigate its antibacterial effect. The results showed that NCBP1 could kill *S. cohnii* L5 rapidly within 1 hour after 4× MIC of NCBP1 treatment. Moreover, at the levels of 10× MIC, NCBP1 killed bacteria within 20 min, exhibiting higher efficacy than vancomycin (Fig. 2B and fig. S4). Altogether, these findings demonstrate the rapid bactericidal activity of NCBP1 against *S. cohnii*.

To decipher the structure-activity relationship of NCBP1, we analyzed its secondary structure by circular dichroism (CD) spectroscopy using sodium dodecyl sulfate (SDS) and 2,2,2-trifluoroethanol (TFE), which are commonly used to simulate membrane environments (*31*, *32*). The result showed that wherever in phosphate-buffered saline (PBS), SDS, or TFE, NCBP1 mainly adapted the dominant configuration of a random coil (Fig. 2C). Nevertheless, NCBP1 showed a slight red shift from 200 to 205 nm with an increased molar ellipticity in negatively charged SDS compared with that in PBS (Fig. 2C). Accordingly, we suspect that NCBP1 targets *S. cohnii* through electrostatic interaction due to its intrinsic two positively charged amino acids. To assess the potency of these positive charges, we synthesized a series of derivatives with alanine (Ala) replacement of the positively charged Lys^1 and Arg^5 (Fig. 2D and fig. S5). The derivatives with either Lys^1 (NCBP1a) or Arg^5 (NCBP1b) replacement lost antibacterial activity (MICs >512 μM) (Fig. 2, E and F, and table S6). Similarly, the replacement of both Lys^1 and Arg^5 (NCBP1c) resulted in the loss of antibacterial activity as well. Collectively, these results suggest that the positively charged amino acid residues are essential for the antibacterial activity of NCBP1.

NCBP1 displayed bactericidal activity by targeting bacterial membrane

In view of the rapid bactericidal activity of cationic NCBP1, we speculated that NCBP1 might target bacterial membranes. To test it, we first determined the activity of NCBP1 in the presence of various phospholipids, the major components of bacterial membranes. Compared to cationic phosphatidylethanolamine (PE) and phosphatidylcholine (PC), the exogenous addition of anionic PG and CL totally abolished the activity of NCBP1 (Fig. 3, A and B). Correspondingly, the MIC of NCBP1 showed a dose-dependent increase in the presence of PG or CL, particularly for exogenous PG (Fig. 3C). Furthermore, we performed microscale thermophoresis (MST) analysis to investigate the selective interaction between NCBP1 and PG. We observed a high binding affinity between NCBP1 and PG, with the equilibrium dissociation constant (K_d) of 5.34 μM, whereas there was no binding for PE (Fig. 3D). Altogether, these findings suggest that the bactericidal activity of NCBP1 may be exerted through a membrane-targeting mechanism.

To further test this hypothesis, we conducted a calcein dye leakage assay using phospholipid vesicles that mimic bacterial membranes (*33*, *34*). The results demonstrated that NCBP1 induced concentration-dependent dye leakage (Fig. 3E), suggesting that NCBP1 disrupts the bacterial membrane to exert its antibacterial effect. Moreover, we then examined the membrane permeability by monitoring the uptake of propidium iodide (PI) in *S. cohnii* L5. It showed a dose-dependent increase of fluorescence under the treatment of NCBP1 (Fig. 3F), denoting the damage of bacterial membranes. Consistently, the proportion of dead bacteria increased gradually with increasing concentrations of NCBP1 (Fig. 3G), based on the stained assay with the probes of Calcein-AM and PI (*35*). In addition, we used scanning electron microscopy (SEM) and transmission electron microscopy (TEM) to evaluate the surface morphology and subsequent intracellular structure changes caused by NCBP1 at 30, 60, 180, and 240 min. To achieve

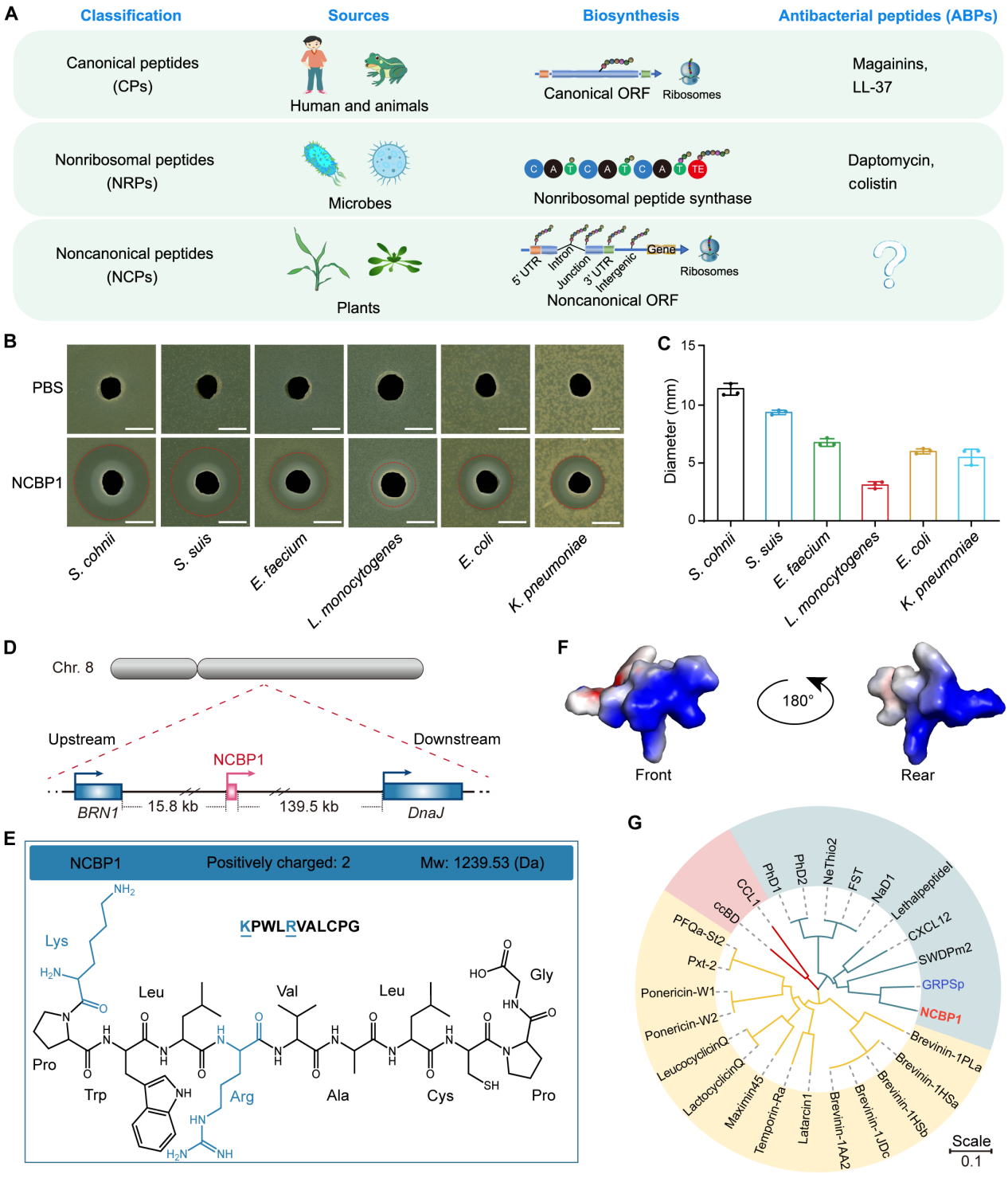

Fig. 1. Noncanonical antibacterial peptides in maize. (**A**) Classification of ABPs. (**B**) Broad-spectrum antibacterial activity of NCBP1. Agar diffusion assay of NCBP1 (0.4 μmol per disk) against MDR bacterial strains. The inhibition zones of NCBP1 are shown in red circles. Scale bars, 5 mm. (**C**) The corresponding inhibition zone diameters of NCBP1. Data are presented as mean ± SDs ($n = 3$ biological replicates). (**D**) The location of NCBP1 derived from maize genome. The distances between NCBP1 (red) and the adjacent genes (blue, *BRN1* and *DnaJ*) are shown between two black dotted lines. The start site of NCBP1 and the direction of transcription of the adjacent genes are indicated by arrows. (**E**) Chemical structure of NCBP1. Cationic amino acid residues are marked in blue. (**F**) The three-dimensional structure of NCBP1 predicted by AlphaFold2. Positive charges, negative charges, and hydrophobic groups are shown in blue, red, and white, respectively. (**G**) Phylogenetic analysis of NCBP1 orthologous peptides. The phylogenetic tree is constructed using the Construct/Test Neighbor-Joining method. NCBP1 and GRPSp are indicated in red and blue font, respectively. The tree scale is 0.1.

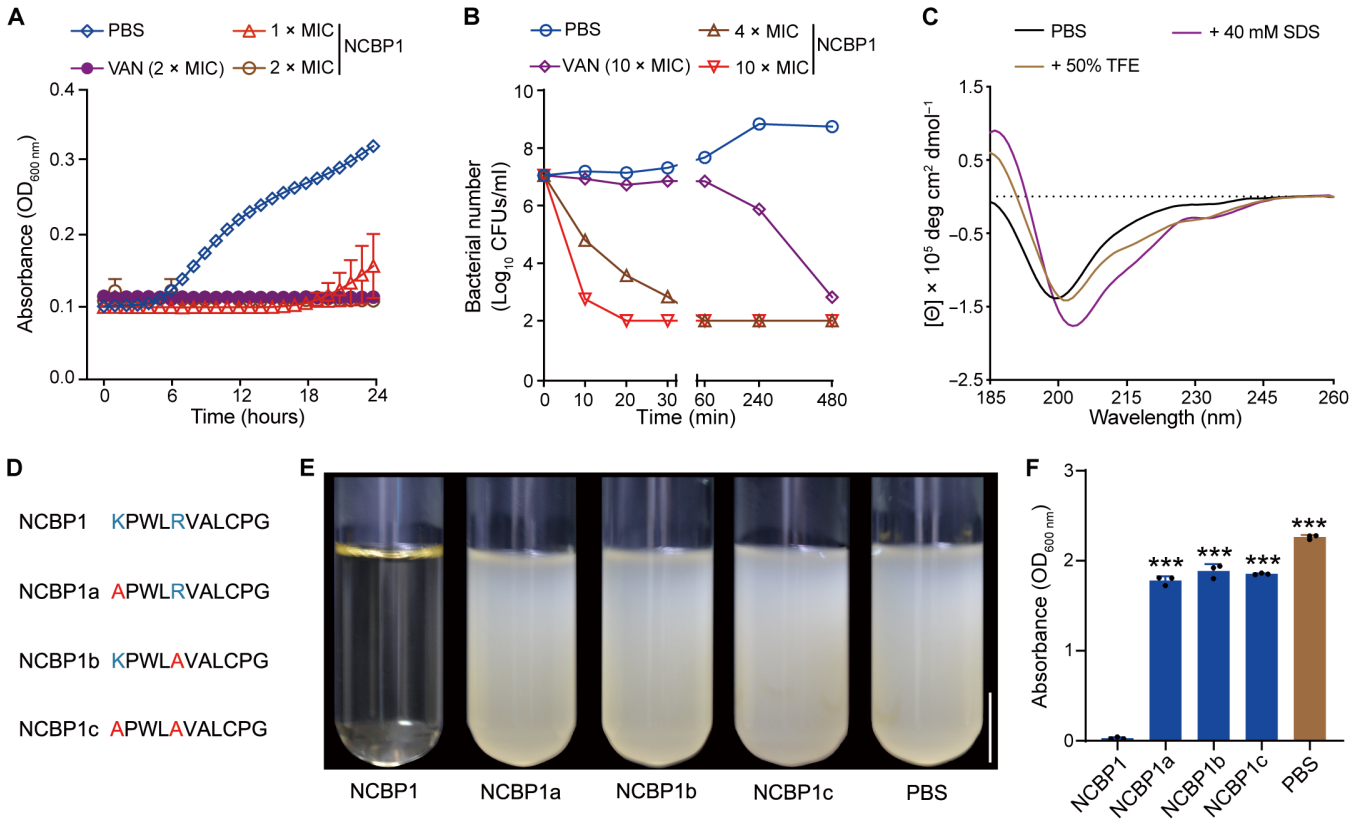

Fig. 2. Rapid bactericidal activity of NCBP1. (**A**) Growth curves of *S. cohnii* L5 in the presence of NCBP1 at 1× and 2× MIC. PBS and vancomycin (VAN, 2× MIC) were used as negative and positive control, respectively. (**B**) Time-killing kinetics of NCBP1 against *S. cohnii* L5 [1 × 10^7 colony-forming units (CFUs)/ml] at 4× and 10× MIC. PBS and VAN (10× MIC) were used as controls. (**C**) Normalized CD spectra of NCBP1 (0.1 mM) in PBS (black), 40 mM SDS (purple), and 50% TFE (yellow). (**D**) Amino acid sequences of NCBP1 derivatives. Cationic amino acid residues are in blue, and alanine is shown in red. (**E**) Antibacterial activities of NCBP1 and the derivatives. Scale bar, 1 cm. (**F**) Bacterial density of *S. cohnii* treated with NCBP1 and derivatives. PBS was used as the control. Data are presented as mean ± SDs ($n = 3$ biological replicates). *P* values were calculated using one-way analysis of variance (ANOVA). ***$P < 0.001$.

an optimal visual representation, a large number of bacteria [1 × 10^{10} colony-forming units (CFUs)/ml] were used in the SEM and TEM experiments. SEM images revealed obvious morphological changes, such as wrinkling of the cell surface and the loss of intracellular contents over time (Fig. 3H). Correspondingly, we observed membrane disruption and subsequent leakage of intracellular content based on TEM analysis as the exposure time increased (Fig. 3H). To extend the generality of our observations, we found that NCBP1 induced similar cell damage in other bacterial species including both Gram-positive *E. faecium* and *L. monocytogenes*, and Gram-negative *E. coli* (fig. S6). These outcomes provide further evidence that NCBP1 is a membrane-targeting antibacterial agent.

Antibacterial mechanism of NCBP1

To further elucidate the mechanism of NCBP1, we examined the sequential cellular responses in bacteria treated with the peptide. Given that membrane homeostasis plays a pivotal role in bacterial survival and other life cycles, we initially evaluated the effect of NCBP1 on membrane potential, which is essential for maintaining membrane homeostasis. To accomplish this, we used the fluorescent probe 3,3′-dipropylthiadicarbocyanine iodide [$DiSC_3(5)$], a dye that exhibits intense fluorescence when the membrane potential is collapsed (*26*). We observed a sharp increase of fluorescence upon the treatment of NCBP1 (Fig. 4A), which indicated the membrane depolarization. Meanwhile, NCBP1 significantly decreased the intracellular levels of adenosine triphosphate (ATP), while concurrently elevating the extracellular ATP levels (Fig. 4B), denoting the leakage of intracellular contents. Moreover, we found that NCBP1 dose-dependently promoted the accumulation of intracellular reactive oxygen species (ROS) (Fig. 4C). These results suggest that NCBP1 may trigger membrane disruption, leading to the loss of membrane potential, ATP leakage, and ROS accumulation.

To gain a deeper understanding of the molecular mechanism of NCBP1, we carried out a global analysis of the RNA expression profiles in *S. cohnii* L5 treated with NCBP1 at 0.5×, 4×, and 10× MIC. Principal components analysis (PCA) showed close clusters of three replicates for each sample with good reproducibility (Fig. 4D). Compared to the untreated group, marked changes in gene expression patterns were observed under NCBP1 treatments. Specifically, 375, 708, and 1616 differentially expressed genes (DEGs) were identified at 0.5×, 4×, and 10× MIC, respectively (fig. S7A). Gene set enrichment analysis (GSEA) was subsequently performed to further assess the changes at transcript levels in response to NCBP1. The results revealed a significant enrichment of membrane-related DEGs at all concentrations, including 0.5× MIC, indicating that NCBP1 influences membrane-related pathways and functions even at sublethal

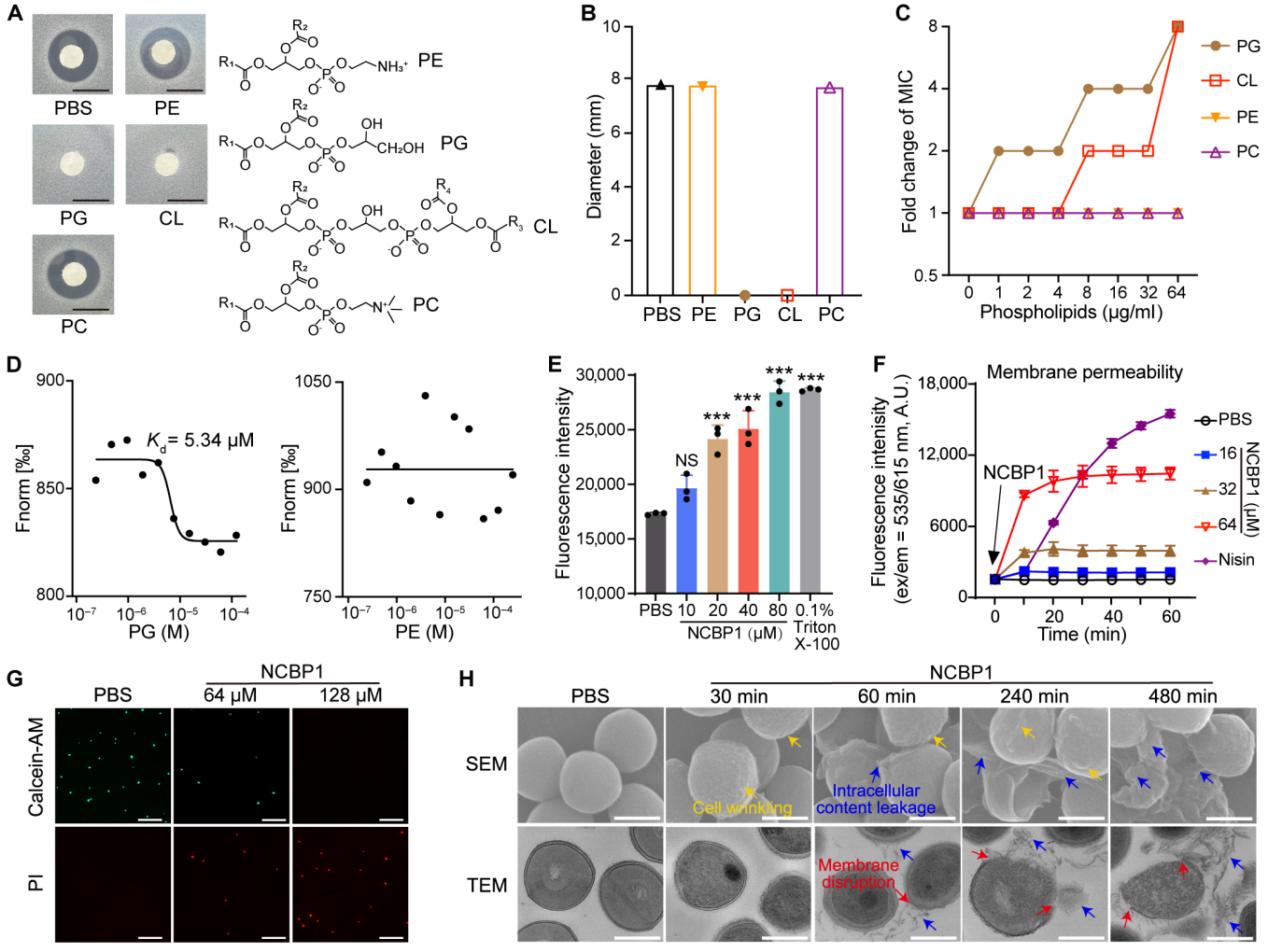

Fig. 3. NCBP1 targeting bacterial membrane. (**A**) Agar diffusion assay of NCBP1 (0.1 μmol) against *S. cohnii* L5 in the presence of PE, PG, CL, and PC (0.25 μmol). The chemical structures of the four phospholipids are shown (right). Scale bars, 10 mm. (**B**) The corresponding inhibition zone diameters (mm) of NCBP1 under the application of phospholipids against *S. cohnii* L5. (**C**) Fold-increased MICs of NCBP1 against *S. cohnii* L5 in the presence of phospholipids (0 to 64 μg/ml) using checkerboard microdilution assays. (**D**) MST analysis of the interaction between NCBP1 and PG (left) and PE (right). The equilibrium dissociation constant (K_d) value is shown. (**E**) Leakage of calcein dye from liposome that mimics bacterial membrane after treatment of NCBP1. Triton X-100 was used as a positive control. (**F**) Dynamic curves of the membrane permeability probed with PI for *S. cohnii* L5 under NCBP1 treatments. Experiments were performed as three biologically independent replicates. Nisin served as the positive control, and PBS was used as the negative control. (**G**) Fluorescence images of *S. cohnii* L5 under NCBP1 treatments. The live cells are stained green by Calcein-AM, whereas the dead cells are stained red by PI. Scale bars, 10 μm. (**H**) Morphological changes in *S. cohnii* L5 (1×10^{10} CFUs/ml) using SEM and TEM under the treatments of NCBP1 (160 μM) for 30, 60, 240, and 480 min. PBS was used as the control. The arrows indicate membrane disruption (red), the leakage of intracellular contents (blue), and the wrinkling of cell surface (yellow), respectively. Scale bars, 0.5 μm. Data are presented as mean ± SDs ($n = 3$ biological replicates). *P* values were calculated using one-way ANOVA. NS, no significance; ***$P < 0.001$.

concentrations (Fig. 4E), consistent with the aforementioned results that the cell membrane is the primary target of NCBP1 (Fig. 3).

In addition, we found that 150 DEGs were significantly induced at both 4× and 10× MIC of NCBP1, while 167 DEGs were inhibited (fig. S7B and table S7). Among those, the representative up-regulated DEGs were primarily categorized into the membrane repair pathway (*fapR*, *yclN*, *relA*, and *azlC*) and stress responses (*ndoA*, *trmR*, and *tcaR*) (Fig. 4F and fig. S7, C and D). For instance, the transcription factor *fapR* involved in the global regulation of membrane lipid biosynthesis (*36*) was significantly up-regulated (fig. S7D), implying a compensatory response to maintain the stability and integrity of bacterial membranes. In addition, the down-regulated genes were mainly associated with the network of energy metabolism (Fig. 4F and fig. S7, C and D). Markedly, the gene *gapB* encoding glyceraldehyde-3-phosphate dehydrogenase, which is required for cellular energy homeostasis by manipulating ATP production (*37*), was significantly down-regulated (fig. S7D). It is consistent with the decreased levels of intracellular ATP in bacteria due to membrane rupture under treatment with NCBP1 (Fig. 4B). To confirm the expression levels of DEGs, five key genes were further analyzed using quantitative reverse transcription polymerase chain reaction (qRT-PCR). The relative expression levels of these genes were consistent with the RNA sequencing (RNA-seq) results (fig. S8), which validate the reliability of the RNA-seq data. Together, these results indicate that NCBP1 significantly

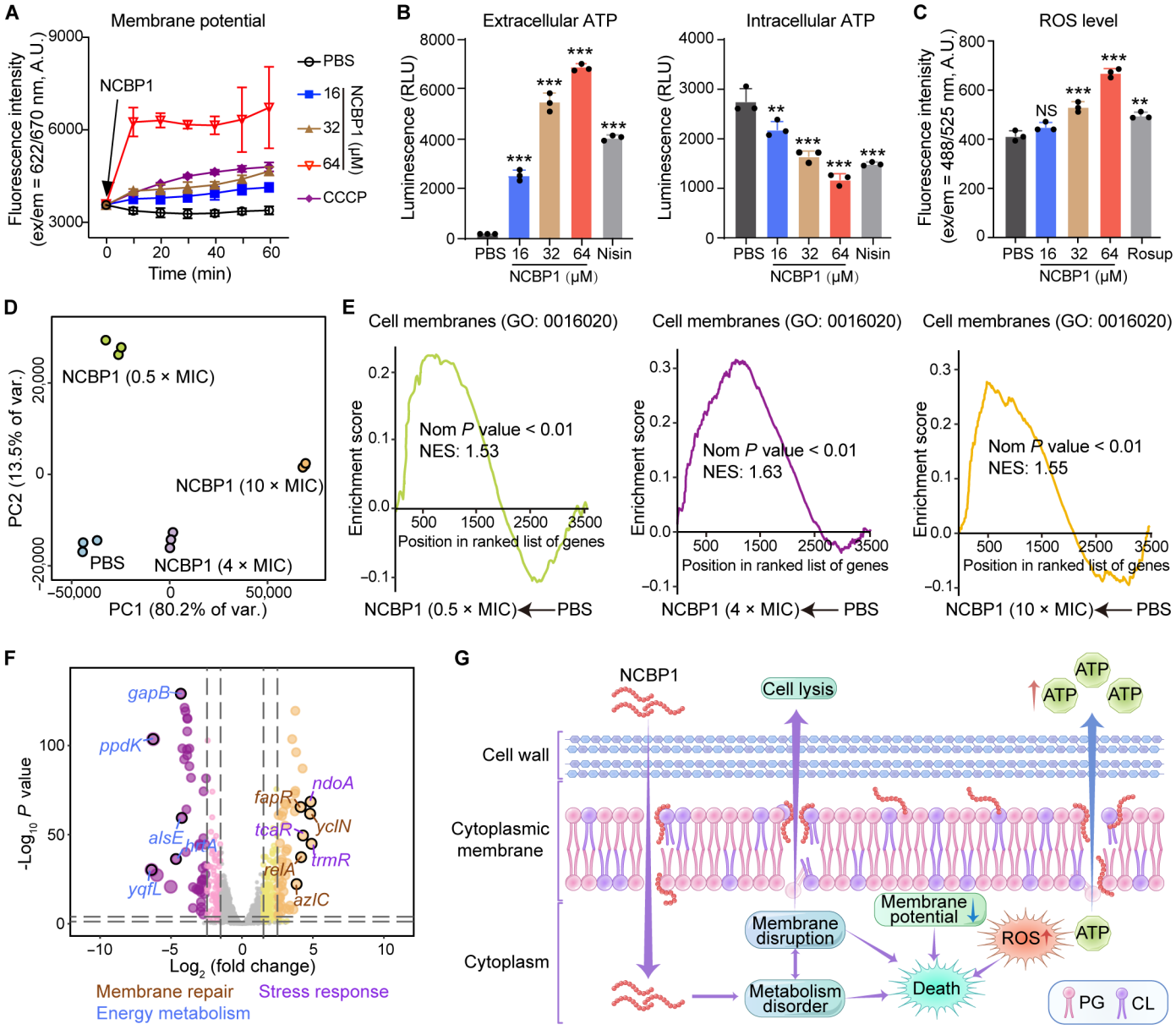

Fig. 4. Mechanism of action of NCBP1 on bacterial membrane disruption. (**A**) Membrane potential of *S. cohnii* L5 treated with NCBP1 (16, 32, and 64 μM). Carbonyl cyanide 3-chlorophenylhydrazone (CCCP) and PBS were used as a positive and a negative control, respectively. (**B**) Extracellular (left) and intracellular ATP level (right) in *S. cohnii* L5 treated with NCBP1, with Nisin as the positive control and PBS as the negative control. (**C**) Total cellular ROS content in *S. cohnii* L5 cells treated with NCBP1. Rosup was used as a positive control, and PBS was used as a negative control. (**D**) PCA of *S. cohnii* L5 under the treatment of NCBP1 at 0.5× MIC (green), 4× MIC (purple), and 10× MIC (yellow) based on RNA-seq analysis. (**E**) GSEA plot of the genes related to the membrane under 0.5× (left), 4× (middle), and 10× MIC (right) of NCBP1 treatments. GO, gene ontology; NES, normalized enrichment score; NOM *P* value, normalized *P* value. (**F**) Volcano plot for the genes in *S. cohnii* L5 treated with 4× MIC of NCBP1. Expressed genes with fold changes of more than 16 under both treatments (4× and 10× MIC) of NCBP1, are marked in yellow (membrane repair), purple (stress response), and blue (energy metabolism). (**G**) Scheme of the mode of action of NCBP1. NCBP1 rapidly kills bacteria by directly causing membrane dysfunction. Data are presented as mean values ± SDs ($n = 3$ biological replicates). *P* values were calculated using one-way ANOVA. $^{**}P < 0.01$, $^{***}P < 0.001$.

induces perturbations to bacterial gene expression and combats bacteria by damaging the cell membrane accompanied by the disruption of cellular metabolism.

Collectively, our results suggest that NCBP1 may exert its bactericidal activity through a mechanism involving membrane disruption, potentially by targeting PG and CL. This disruption may trigger a cascade of events, including the loss of membrane potential, decreased intracellular ATP levels, efflux of extracellular ATP, accumulation of intracellular ROS, and metabolic perturbations (Fig. 4G). Overall, these findings indicate that NCBP1's antibacterial activity is likely driven primarily by its membrane-targeting effects.

NCBP1 showed high safety and excellent stability

Safety and stability are crucial factors that determine the in vivo efficacy and production feasibility of a candidate. Various types of mammalian cells, including sheep red blood cells (RBCs), Vero,

HEp-2, A549, and H9c2 cells, were used to evaluate the cytotoxicity of NCBP1 in vitro. The hemolysis assay indicated that NCBP1 displayed no noticeable hemolytic activity toward RBCs at all concentrations tested (0 to 512 μM) (Fig. 5A). In addition, quantitative cell viability assessments revealed that NCBP1 displayed negligible toxicity toward all mammalian cells, even at the highest concentration tested (512 μM) (Fig. 5B). These results suggest that NCBP1 exhibits favorable safety profiles for mammalian cells in vitro. Furthermore, we conducted in vivo assays to further evaluate the safety of NCBP1 by administering intraperitoneal injections of NCBP1 in mice at three doses (50, 100, and 150 mg/kg). The survival rate of the NCBP1-treated mice remained at 100% after 5 days, even at the highest dose of 150 mg/kg (Fig. 5C), suggesting that NCBP1 has no appreciable toxicity and is safe for in vivo application. Moreover, NCBP1 was able to efficiently maintain its antibacterial activity after exposure to 100°C for 1 and 2 hours (Fig. 5D) and was resistant to a wide range of pH values (pH 2 to 12 for 1 and 2 hours) (Fig. 5E). These results collectively imply that NCBP1 exhibits favorable safety, excellent thermal and pH stability, and has great potential as an antibacterial agent for further development.

NCBP1 protected mice from *S. cohnii* infection

To investigate the in vivo efficacy of NCBP1 as a therapeutic agent for treating bacterial infections, a mouse skin infection model and mouse peritonitis-sepsis model were established using *S. cohnii* L5 as the challenge pathogen. First, we evaluated the in vivo efficacy of NCBP1 in a mouse skin infection model, in which each mouse was inoculated with a high bacterial load of 1×10^7 CFUs. After 1 hour, we dropped NCBP1 or vancomycin into the wound. To evaluate the effect of NCBP1 on wound healing, the area of the wound was recorded every 2 days over a 10-day posttreatment period, and the bacterial burden in the wound was measured through a survival cell count assay of excised wound tissue at day 10 posttreatment (Fig. 5F). The results demonstrated a progressive reduction in wound areas in the NCBP1 groups, with a significantly higher wound healing rate compared to the PBS group (Fig. 5, G and H). By the 10th day, the wounds treated with NCBP1 were nearly healed (Fig. 5, G and H). In addition, NCBP1 treatment significantly reduced the bacterial burden in the wound (fig. S9A). We also observed a significant decrease in bacterial numbers in the liver of NCBP1-treated mice (fig. S9B). NCBP1 did not affect the normal growth of the mice (fig. S9C), supporting the absence of systemic toxicity in vivo.

To further assess the extent of wound healing in the skin, histological analysis was conducted using hematoxylin and eosin (H&E) staining. The results revealed that the wound sizes in the NCBP1 group were obviously reduced compared to the PBS group (fig. S9D). Moreover, NCBP1 demonstrated superior efficacy compared to vancomycin, as evidenced by a smaller wound size in mice treated with NCBP1. Subsequently, collagen deposition, an important indicator of wound healing, was observed by Masson staining experiments, which stained collagen fibers in blue. We found that collagen was fully deposited and densely arranged in the NCBP1 group (fig. S9D), further indicating the accelerated wound healing and great therapeutic effect of NCBP1 in vivo.

Subsequently, we examined the ability of NCBP1 to protect mice from a lethal challenge of *S. cohnii* L5 in a mouse peritonitis-sepsis model. Each mouse was infected with a high bacterial load of 2×10^9 CFUs via intraperitoneal injection. One hour postinfection, NCBP1 or vancomycin was administered intraperitoneally to rescue the mice (Fig. 5F). To evaluate the effect of NCBP1, the survival rate of the mice was recorded every 12 hours over a 72-hour postinfection period, and the bacterial burden in the organs was measured using a survival cell count assay on excised organs (Fig. 5F). In this model, nearly 90% of mice died after infection with *S. cohnii* for 36 hours (Fig. 5I). NCBP1 (110 mg/kg) rescued all the mice (100%), similar to vancomycin. Furthermore, NCBP1 significantly reduced bacterial burden in major organs, including the heart, liver, spleen, lung, and kidney (Fig. 5J). Together, these results demonstrate the potential of NCBP1 to treat *S. cohnii* infections in vivo.

NCBP1 enhances resistance to fungal diseases in maize plants

Given that plant fungal pathogens consistently cause substantial economic losses in agricultural production around the world, we further explored the antifungal effect and disease resistance of NCBP1 against these pathogens. We first tested the antifungal activity of NCBP1 against *Bipolaris maydis*, *Fusarium verticillioides*, *Curvularia lunata*, and *Fusarium proliferatum*, which are responsible for severe fungal diseases in cultivated crops (*38*). The results demonstrated that NCBP1 effectively inhibited fungal growth (Fig. 6, A to D, and fig. S10). Considering the role of positive charge in antibacterial efficacy, we investigated whether antifungal activity might also be attributed to the positive charge. To verify this, we tested the effects of NCBP1 and its derivatives in which Lys^1 (NCBP1a), Arg^5 (NCBP1b), or both residues (NCBP1c) were replaced with alanine (Ala), against two fungal pathogens, *B. maydis* and *C. lunata*. The results demonstrated that NCBP1a, NCBP1b, and NCBP1c caused a notable increase in hyphal diameters and a significant decrease in inhibition rates for both *B. maydis* and *C. lunata* compared to NCBP1-treated controls (fig. S11). Collectively, these results indicate the importance of the positively charged amino acid residues in maintaining the antifungal activity of NCBP1.

To further evaluate NCBP1's impact on disease resistance in maize, we focused on *B. maydis* and *F. verticillioides*, the causative agents of southern corn leaf blight (SCLB) and seed rot, respectively (*39*, *40*). Maize plants treated with NCBP1 exhibited markedly reduced SCLB lesions compared to controls (Fig. 6, E and F), and the DNA content of *B. maydis* was significantly lower in the treated plants (Fig. 6G). At the cellular level, cross sections of *B. maydis*–infected leaves revealed fewer fungal hyphae and less damage in NCBP1-treated plants, whereas extensive hyphal growth and cell destruction were observed in the control group (fig. S12A). These results suggest that NCBP1 could enhance resistance to SCLB. Similarly, seeds inoculated with *F. verticillioides* showed slower symptom progression and reduced fungal growth in the NCBP1-treated group (Fig. 6H). Both the mycelial size and DNA content of *F. verticillioides* were significantly reduced in treated seeds (Fig. 6, I and J). Furthermore, NCBP1 treatment markedly decreased fumonisin contamination in seeds (fig. S12B), indicating that NCBP1 can inhibit the infection of *F. verticillioides* and enhance resistance to seed rot. Together, these results demonstrate that NCBP1 treatment enhances broad-spectrum disease resistance in maize.

DISCUSSION

With the emergence of technological advancements, the existence of thousands of NCPs throughout the genome, including intergenic regions, 5′UTRs, 3′UTRs, introns, and junctions, has been discovered

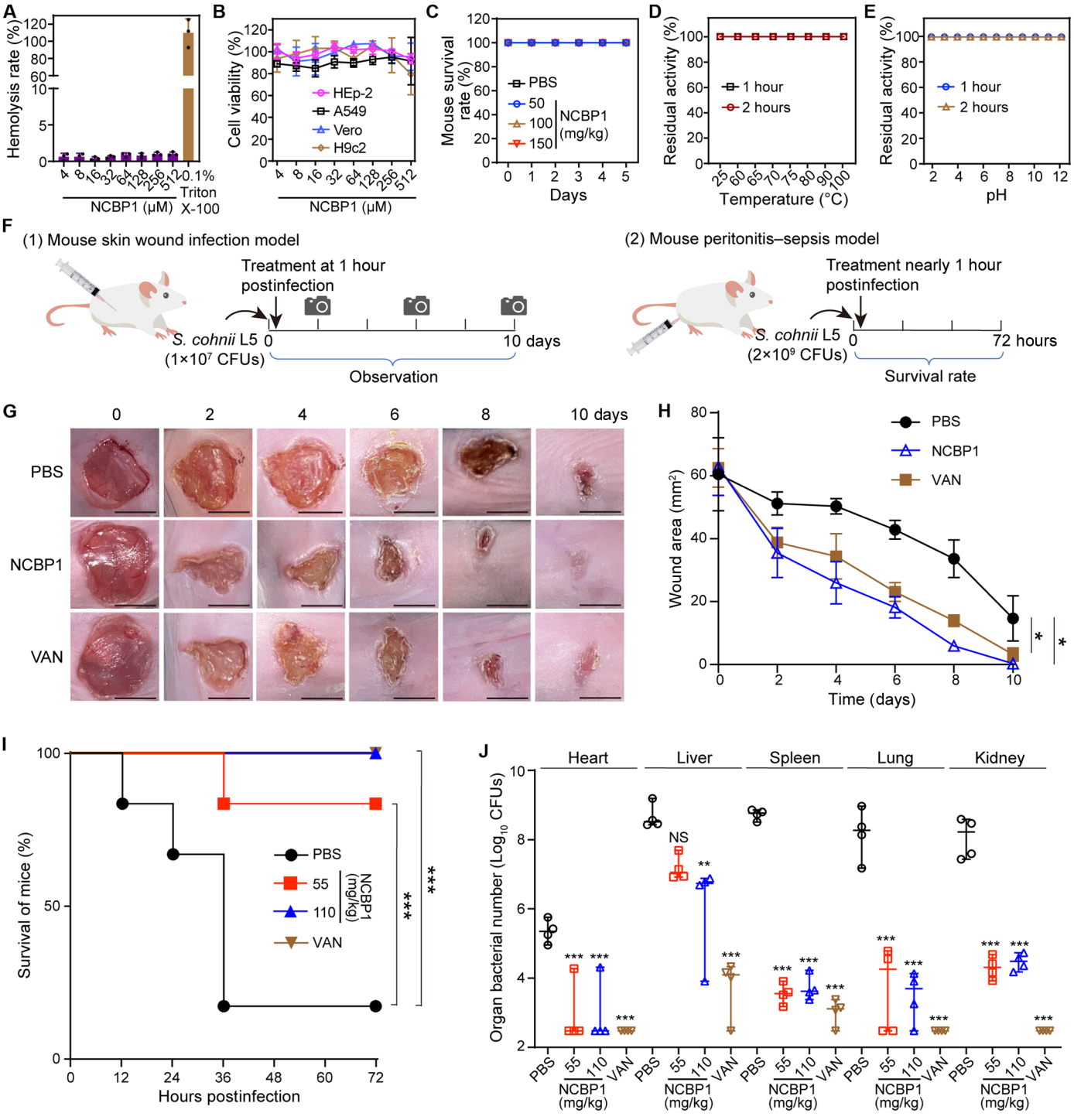

Fig. 5. Safety and antibacterial properties of NCBP1 in vivo. (**A**) Hemolytic activity of NCBP1. Triton X-100 was used as a positive control. Data are presented as mean ± SDs ($n = 3$ biological replicates). (**B**) Cell viability of HEp-2, A549, Vero, and H9c2 cells treated with NCBP1 based on the water-soluble tetrazolium salt-1 (WST-1) assay. (**C**) Survival rates of the mice after 5 days ($n = 5$ mice per group) following intravenous injections of PBS or NCBP1 at doses of 50, 100, and 150 mg/kg. (**D**) Residual antibacterial activity of NCBP1 at temperatures ranging from 25° to 100°C for 1 and 2 hours. *S. cohnii* L5 was used as the tested strain. (**E**) Residual antibacterial activity of NCBP1 at different pH levels ranging from 2 to 12 at 37°C for 1 and 2 hours. (**F**) Scheme of the experimental protocol of the mouse skin wound infection model and mouse peritonitis-sepsis model. (**G**) Representative images of the wounds. Scale bars, 5 mm. (**H**) Changes of wound areas under the treatment of NCBP1 on days 2, 4, 6, 8, and 10. (**I**) Survival rates of mice in the peritonitis-sepsis model ($n = 6$). *P* values were calculated using the two-sided log-rank (Mantel-Cox) test. (**J**) Effect of NCBP1 (55 and 110 mg/kg) or vancomycin (VAN, 110 mg/kg) on bacterial survival in different organs of mice ($n = 4$). *P* values were calculated using one-way ANOVA. $^{*}P < 0.05$, $^{**}P < 0.01$, $^{***}P < 0.001$.

(*22*, *24*). NCPs have caught important attention as functionally important endogenous peptides in various organisms, participating in key biological processes such as calcium transport (*41*), embryogenesis (*42*), muscle performance (*43*, *44*), translation control (*23*, *45*, *46*), and immune response (*47*) in animal and human, as well as root development (*48*), metabolite synthesis (*49*), and hormone regulation (*50*) in plants. However, the antibacterial potential of plant-derived NCPs and their underlying mechanisms have yet to be studied. Here, we screened a library of NCPs derived from maize and identified an NCP NCBP1 with broad-spectrum antibacterial activity against MDR bacteria (Fig. 1, B and C, and fig. S1). Unlike LL-37, which is a well-known ABP derived from a canonical ORF in humans (*51*), and colistin, a nonribosomal peptide synthesized by bacteria (*52*), NCBP1 is a distinct ABP derived from a noncanonical ORF in plants, highlighting its unique origin and potential for innovative biological functions. Structurally, NCBP1 is a short linear peptide with only a single cysteine residue, distinguishing it from most canonical and conventional ABPs in plants, which are typically rich in cysteine (*53*). Our findings provide an additional source for the discovery of unexplored antibacterial agents against MDR bacteria. However, it is important to note that further molecular modifications, such as peptide sequence optimization, cyclization to enhance stability, and combination therapy to achieve synergistic effects, may be necessary to improve the antibacterial activity of NCBP1. These adjustments could expand its potential application against MDR pathogens.

Compared to vancomycin, NCBP1 exhibits an advantage over this clinically used antibiotic, with faster time-killing dynamics that can kill bacteria within 10 min (Fig. 2B). Such a rapid killing rate can reduce bacterial survival and growth, further diminishing the emergence of antibiotic resistance (*26*). Unlike existing antibiotics that target specific enzymes or proteins (*54*, *55*), NCBP1 likely kills bacteria by interacting with anionic phospholipids in bacterial membranes, such as PG and CL (Fig. 3), which may result in structural and functional damage to bacterial membranes. This mode of action of NCBP1 will offer less potential to develop antibiotic resistance, because it targets a fundamental structure of the bacterial cell, membrane phospholipids, that cannot be easily modified or altered by the bacteria to evade the effects of the antibiotic. Specifically, the anionic PG is a predominant phospholipid in bacteria (*56*), which may account for the broad-spectrum antibacterial activity of NCBP1. This membrane-dependent mechanism was further supported by the accumulation of ROS levels. It has been reported that ROS production in bacteria following exposure to ABPs has been linked to their membrane-damaging mechanism (*57*).

The application of plant-derived ABPs against MDR bacteria has been persistently ignored, probably due to the low stability and poor bioavailability in vivo (*58*). In this study, we found that NCBP1 showed excellent stability under harsh conditions and did not display observable hemolysis or cytotoxicity to mammalian cells and mice (Fig. 5, A to E). Localized infections, such as skin wound infections, are challenging due to limited blood flow to these areas and the presence of necrotic tissue (*59*). We evaluated the therapeutic potential of NCBP1 against *S. cohnii*, a pathogen associated with skin wound infections. The results revealed that NCBP1 had a remarkable impact on reducing the wound area and bacterial load caused by *S. cohnii*. Moreover, when applied topically, NCBP1 exhibited comparable efficacy to vancomycin (Fig. 5, G to J). These results suggest that plant-derived ABPs are an innovative and safe source for the discovery and development of therapies against MDR pathogens.

In parallel to what has occurred in medicine, antimicrobial peptides have also been proposed for potential use in agriculture (*60*). Plant diseases, especially caused by a variety of fungal pathogens, lead to substantial reduction in crop yield and threaten food security worldwide (*28*, *38*). Maize is one of the most important crop species widely used for human consumption and animal feed. Moreover, maize serves as a key model organism for plant biological research due to its remarkable genetic diversity (*61*). The B73 inbred line, in particular, is extensively studied and has a well-sequenced genome, making it an ideal choice for a wide range of plant studies. In this study, NCBP1 not only inhibited fungal growth but also enhanced broad-spectrum resistance to fungal diseases in maize (Fig. 6). These findings also underscore its potential as an innovative antifungal candidate for agricultural applications. In addition to its ability to target MDR bacterial strains (Fig. 1, B and C), this further highlights NCBP1's dual functionality, positioning it as a promising candidate for applications in both agriculture and medicine.

In conclusion, we identified an NCP NCBP1, with broad-spectrum antibacterial activities through targeting bacterial membranes. Moreover, NCBP1 exhibited promising efficacy against *S. cohnii* infection in vivo, with desirable stability and safety in both mammalian cells and mice. Furthermore, NCBP1 treatment enhances resistance to a broad spectrum of fungal diseases in maize. These findings demonstrate that NCBP1 is a promising candidate for the development of alternative therapies against MDR bacterial infections and for enhancing resistance to plant fungal diseases. Our study represents the initial discovery of the antimicrobial potential of plant-derived NCPs, providing an untapped source for the discovery of antimicrobial agents.

MATERIALS AND METHODS

Experimental design

In this study, we aimed to investigate the efficacy of plant-derived NCPs in combating MDR bacterial infection. This study consists of four major steps. First, a homemade library of NCP in maize was used to screen and a broad-spectrum ABP named NCBP1 was identified. Second, the target of NCBP1 was identified, and the mechanism of combating MDR bacteria was explored. In the third step, the therapeutic potential of NCBP1 was evaluated in vivo using a mouse wound infection model and a peritonitis-sepsis model. Last, the antifungal effect and disease resistance of NCBP1 against plant fungal pathogens were further explored. This four-step experimental design was intended to provide a comprehensive understanding of the role of plant-derived NCPs in treating MDR bacterial infections, with the hope of contributing to the development of alternative therapies in the future.

Functional studies were performed in vivo using mouse models to determine whether NCBP1 was a potential therapeutic candidate for treat *S. cohnii* infections. For all animal studies, subjects were assigned randomly to groups. Animal or sample allocation and data acquisition were performed in a blinded manner. No data were excluded from analyses.

Synthesis of maize NCPs

The peptide library was constructed based on our previous study (*22*), in which we initially identified 1993 maize endogenous peptides. From this dataset, the top 1000 peptides were selected based on their peptide scores, which serve as indicators of peptide quality. These

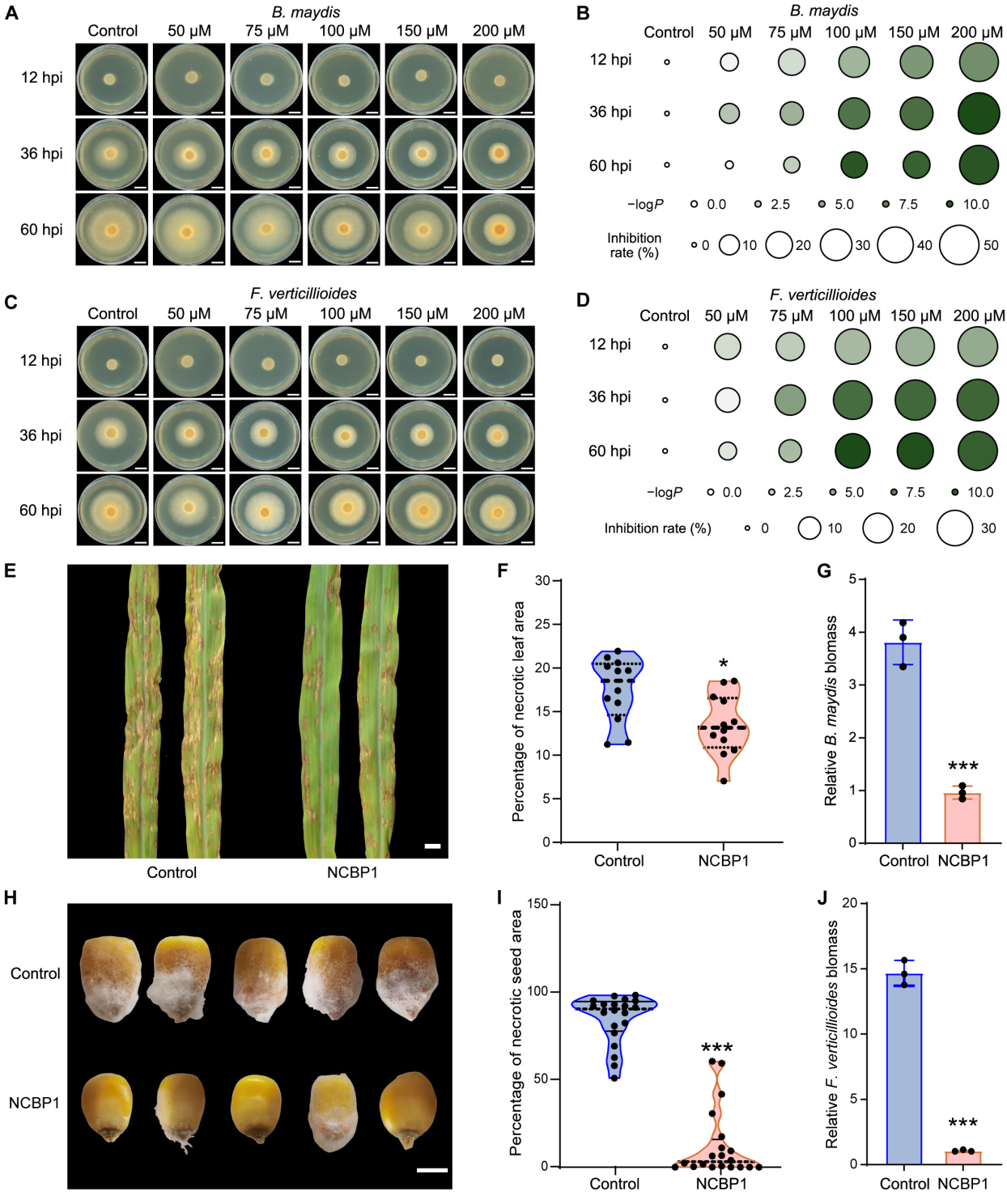

Fig. 6. NCBP1 enhances broad-spectrum disease resistance in maize. (**A**) Images of *B. maydis* treated with 0 (control), 50, 75, 100, 150, and 200 μM NCBP1 at 12, 36, and 60 hours postinoculation (hpi). Scale bars, 5 mm. (**B**) The inhibition rates (%) of NCBP1 on *B. maydis* after 36 hours of treatment at concentrations of 0 (control), 50, 75, 100, 150, and 200 μM. (**C**) Images of *F. verticillioides* treated with 0 (control), 50, 75, 100, 150, and 200 μM NCBP1 at 12, 36, and 60 hpi. Scale bars, 5 mm. (**D**) The inhibition rates (%) of NCBP1 on *F. verticillioides* after 36 hours of treatment at concentrations of 0 (control), 50, 75, 100, 150, and 200 μM. (**E**) Representative images of southern corn leaf blight caused by *B. maydis* in NCBP1-treated and control plants. Photos were taken 4 days after inoculation (DAI). Scale bar, 1 cm. (**F**) Statistical analysis of the percentage of necrotic leaf area in NCBP1-treated and control plants infected with *B. maydis*. (**G**) Quantification of *B. maydis* DNA in NCBP1-treated and control plants. Maize *Ef1a* was used as the internal control. (**H**) Representative images of seed rot caused by *F. verticillioides* in NCBP1-treated and control plants. Photos were taken at 7 DAI. Scale bar, 0.5 cm. (**I**) Statistical analysis of the percentage of diseased seed area in NCBP1-treated and control plants infected with *F. verticillioides*. (**J**) Quantification of *F. verticillioides* levels in the seeds by quantitative PCR. Maize *Ef1a* was used as the internal control. *P* values were calculated using Student's *t* test. $^{*}P < 0.05$, $^{***}P < 0.001$.

peptides and NCBP1's derivatives were synthesized using an Fmoc (9-fluorenyl methoxycarbonyl)–based solid-phase peptide synthesis method (GL Biochem, Shanghai, China). Briefly, the carboxyl group of the first Fmoc-protected amino acid at the C terminus was connected with the insoluble polymer resin. Then, the Fmoc protective group was removed using hexahydropyridine, and the C terminus of the second amino acid was linked to the N terminus of the first amino acid at the alpha position through peptide bond formation. The remaining amino acids were added in sequence using the same process. Last, the synthesized peptides were eluted from the resin using trifluoroacetic acid. Detailed information on these peptides can be found in table S1. All amino acids used in this study were natural L-type amino acids with a purity greater than 90%.

Cell lines and bacterial strains

All the strains (table S2) were grown in brain heart infusion (BHI, Hopebio, Qingdao, China, HB8297-5) broth or on BHI agar plates at 37°C. Additional fetal bovine serum (FBS, Every Green, Hangzhou, China, 13011-8611) was added for *S. suis* SC181. Four mammalian cell lines were used in this study, which were obtained from the American Type Culture Collection (ATCC), including African green monkey kidney cells (Vero, ATCC CCL-81), human epidermoid carcinoma cells (HEp-2, ATCC CCL-23), lung carcinoma cells (A549, ATCC CCL-185), and rat cardiomyocyte cells (H9c2, ATCC CRL-1446). These cells were cultured in Dulbecco's modified Eagle's medium (DMEM, Gibco, Carlsbad, USA, C11995500BT) supplemented with 10% heat-inactivated FBS (Invitrogen, Carlsbad, USA, 10270106), 1% (w/v) penicillin-streptomycin (Sigma-Aldrich, St. Louis, USA, P4333-20ML), and 1% (w/v) sodium pyruvate (Sigma-Aldrich, St. Louis, USA, P4562-5G) at 37°C in a 5% CO_2 atmosphere. The mammalian cells were characterized using short tandem repeat genotyping before testing and were confirmed to be free of Mycoplasma contamination through PCR detection using the Mycoplasma PCR Detection Kit (Beyotime, Shanghai, China, C0301S).

Animals used in the study

Female BALB/c mice aged 6 to 8 weeks (weighed 18 to 20 g) were obtained from SPF Beijing Biotechnology Co. Ltd. (Beijing, China). All mice were adapted to standardized environmental conditions of 23° ± 2°C and 55 ± 10% humidity for 1 week before infection. The experimental protocols were approved by the Laboratory Animal Ethics Committee of China Agricultural University (AW01202202-2-1), and the laboratory animal usage license (SYXK-2021-0012) was certified by Beijing Association for Science and Technology.

Primary screening of maize ABPs

Maize peptides with antibacterial activity were screened using different MDR bacterial cultures including *S. cohnii* L5, *E. faecium* E1077, *L. monocytogenes* NH1, *S. suis* SC181, *K. pneumoniae* B, or *E. coli* MLS9F, with a final concentration of 1.5×10^4 CFUs/ml. The peptides were diluted to a final concentration of 200 μM in Mueller-Hinton Broth (MHB, Hopebio, Qingdao, China, HB6231). After incubation at 37°C for 18 hours, any peptides that could inhibit the bacteria with no visible growth were chosen for further determination of their antibacterial activities.

Agar diffusion assay

MDR bacterial strains including *S. cohnii* L5, *E. faecium* E1077, *L. monocytogenes* NH1, *S. suis* SC181, *K. pneumoniae* B, and *E. coli* MLS9F were used to evaluate the antibacterial activity of NCBP1. Bacteria grown in BHI broth for 12 hours at 37°C were diluted to approximately 1×10^6 CFUs/ml with 0.1 M PBS. Next, 0.05 ml of the diluted bacteria suspensions was spread on 10 ml of BHI agar medium (final concentration of 5×10^3 CFUs/ml). Once the agar plates solidified, a 5-mm plug was removed from the center of the agar plates and NCBP1 was added. The plates were incubated at 37°C for 24 hours, and the zones of inhibition were photographed and measured.

Antibacterial activity analysis

The MICs of NCBP1, its derivatives, and antibiotics were determined using the broth microdilution method, in accordance with the Clinical and Laboratory Standards Institute 2021 guidelines. NCBP1, its derivatives, and antibiotics were diluted twice and then mixed with an equal volume of bacterial suspensions containing approximately 1×10^6 CFUs/ml in a clear ultraviolet-sterilized 96-well microtiter plate. The MIC values were determined as the lowest concentrations that inhibited bacterial growth after 18 hours of incubation at 37°C. In addition, to visually assess their activity, *S. cohnii* L5 was diluted in MHB (approximately 1.5×10^6 CFUs/ml), placed in a glass tube, and treated with NCBP1 or its three derivatives at a concentration of 64 μM for 24 hours. After incubation at 37°C for 24 hours, the cultures were photographed, and the absorbance at $OD_{600\ nm}$ (optical density at 600 nm) was recorded.

Characteristics of NCBP1

The genomic location of NCBP1 was analyzed by aligning its sequence to the B73 reference genome (v4.0). The purity (97.59%) and molecular mass (1239.53 Da) of synthesized NCBP1 were determined by high-performance liquid chromatography (HPLC) and electrospray ionization mass spectrometry, respectively. The chemical structures were drawn using the software ChemDraw 22.0.0.

Prediction of peptide structure

To examine the potential 3D structure of NCBP1 and GRPSp, we used AlphaFold2 (https://colab.research.google.com/github/sokrypton/ColabFold/blob/main/AlphaFold2.ipynb) to predict the 3D structure from peptide amino acid sequence with high accuracy. The electrostatic potential of the peptides was then calculated and visualized using the Automated Parcel Bundle System plugin in PyMOL (Version 2.5.2) (*62*), a popular molecular visualization software. In our visualization, we represented positive potentials in blue and negative potentials in red, with the color scale given in units of kT/e_c.

Phylogenetic analysis

NCBP1 orthologs were selected from the APD3 database (http://aps.unmc.edu/AP/), and their sequences were retrieved. A multiple sequence alignment using Clustal Omega was performed to determine the amino acid sequence similarities between NCBP1 and other ABPs. Homologs were identified using TBLASTP with individual peptides as query sequences under permissive conditions (low-complexity filter inactivated, PAM30 matrix, word size 2, expect value 1000) (*63*). The phylogenetic tree was constructed using the Construct/Test Neighbor-Joining method of MEGA 7.0, with 3000 bootstrap replicates, and evolutionary distances were computed using the *p*-distance method.

Selection of *S. cohnii* L5

S. cohnii L5 was isolated from blood samples in Henan, China, in 2019, and identified as *S. cohnii* through 16S rRNA sequencing (fig. S13 and data S1). MIC testing subsequently confirmed its resistance to chloramphenicol, florfenicol, linezolid, benzylpenicillin sodium, ampicillin, gentamicin, trimethoprim, tetracycline, and erythromycin, classifying it as an MDR pathogen (table S5).

Growth dynamics

For the growth curves of bacteria, we mixed different concentrations of NCBP1 (1× and 2× MIC) or vancomycin (2× MIC) with an equal volume of *S. cohnii* L5 with a turbidity of 1×10^6 CFUs/ml in MHB medium in a 96-well microplate with the plate lid covered. The microplate was incubated at 37°C, and the growth curves were recorded at $OD_{600\,nm}$ every hour for 24 hours using an Infinite M200 Microplate Reader (Tecan, Männedorf, Switzerland).

Time-kill curves

S. cohnii L5 was cultured to exponential phase at 37°C with shaking at 200 rpm and then diluted in MHB to a desired concentration of 1×10^6 to 1×10^7 CFUs/ml. NCBP1 (at final concentrations of 4× and 10× MIC) or vancomycin (at a final concentration of 10× MIC), was added to the cultures, which were then incubated at 37°C with shaking at 200 rpm. To determine the number of live bacteria, 100 μl of *S. cohnii* L5 culture was collected at 10, 20, 30, 60, 240, and 480 min; serially diluted; and plated on Tryptose Soya Agar (TSA, Hopebio, Qingdao, China, HB7026-9) plates. After incubating at 37°C for 24 hours, the CFUs were counted and photographed.

CD spectroscopy

CD measurements on the secondary structure of NCBP1 were carried out using a Chirascan (Applied Photophysics, Leatherhead, England) at a wavelength range of 185 to 260 nm and at 25°C (*64*). The solution was placed in a quartz cylindrical cell with a path length of 0.1 cm (Hellma Analytics, Müllheim, Germany), and spectra were corrected by subtracting the spectrum of buffer background. To mimic the bacterial membrane environment, SDS (Sigma-Aldrich, St. Louis, USA, 436143) and TFE (Sigma-Aldrich, St. Louis, USA, T62003) were added to the solution. The secondary structures of NCBP1 were analyzed using the CDNN software (Version 2.1).

Phospholipid supplement assay

The antibacterial activities of the mixtures of NCBP1 and bacterial membrane compounds including PG (Sigma-Aldrich, St. Louis, USA, 841188P), PE (Sigma-Aldrich, St. Louis, USA, 840027P), CL (Sigma-Aldrich, St. Louis, USA, 841199P), and PC (Sigma-Aldrich, St. Louis, USA, 840051P) were determined using a disk diffusion assay and a checkerboard microdilution assay (*26*). In the disk diffusion assay, mixtures of NCBP1 and phospholipids (at 2.5× molar equivalents) were incubated at 37°C for 30 min and then added to diffusion disks placed on Mueller-Hinton agar (Hopebio, Qingdao, China, HB6232) containing *S. cohnii* L5 (2×10^7 CFUs/ml). The plates were incubated overnight at 37°C, and the inhibition zones were photographed and measured using ImageJ (Version 1.8.0). For the checkerboard microdilution assay, NCBP1 was diluted along the abscissa, while the bacterial membrane compounds were diluted along the ordinate.

Microscale thermophoresis

The equilibrium dissociation constant (K_d) values between NCBP1 and different phospholipids were measured using MST with Monolith NT.115 (Nanotemper Technologies GmbH, München, Germany) as previously described (*65*). Briefly, NCBP1 was serially diluted from 500 μM in 20 mM *N*-2-hydroxyethylpiperazine-*N*-ethanesulfonic acid (Hepes) buffer (pH 7). Then, fluorescent-labeled PG (18:1 to 12:0 NBD-PG, 5 μM) or PE (14:0 to 12:0 NBD-PE, 5 μM) dissolved in Hepes was added to the serial dilutions of NCBP1 (500 to 0.488 μM) in a 1:1 volume ratio. The samples were examined with Monolith NT.115 using a standard treated capillary (MO-K022, Nanotemper Technologies GmbH, München, Germany) with medium MST power and Auto-detect for blue excitation power. K_d values were determined using the Monolith Affinity Analysis K_d fit.

Calcein leakage assay

The 1,2-dioleoyl-sn-glycero-3-phosphoglycerol large unilamellar vesicles (LUVs) were prepared by the thin-film hydration method followed by extrusion (*66*). Briefly, PG (10 mg) was dissolved in 2 ml of a chloroform/methanol solvent mixture, and the solvents were removed under a stream of nitrogen. The resulting thin lipid film was rehydrated with calcein-containing buffer consisting of 70 mM calcein, 150 mM NaCl, and 0.1 mM EDTA and adjusted to pH 7.4. The LUVs were diluted with PBS to 40 μM and mixed with NCBP1 at concentrations of 10, 20, 40, and 80 μM or Triton X-100 (positive control) for 5 min. The leakage of calcein from the LUVs was monitored by measuring the fluorescence intensity at an excitation wavelength of 490 nm and an emission wavelength of 520 nm on a SpectraMax M5 multimode microplate reader.

Membrane permeability assay

Membrane permeability assay was conducted according to a previous study (*26*). Overnight cultures of *S. cohnii* L5 were first washed and then suspended in 0.01 M PBS (pH 7.4) to obtain an $OD_{600\,nm}$ of 0.5. Then, 10 nM PI (Thermo Fisher Scientific, Waltham, USA, P1304MP) was added. After balancing, different concentrations of NCBP1 (16, 32, and 64 μM) were then added, and the fluorescence was recorded every 10 min with the excitation wavelength at 535 nm and emission wavelength at 615 nm by an Infinite M200 Microplate reader (Tecan, Männedorf, Switzerland).

Calcein-AM and PI assays

The viability of *S. cohnii* L5 after treatment of NCBP1 was assessed using a Calcein-AM/PI double staining kit (Yeasen, Shanghai, China, 40747) according to the manufacturer's instructions. Briefly, cultures of *S. cohnii* L5 were adjusted to an $OD_{600\,nm}$ of 0.5 and treated with NCBP1 (64 and 128 μM) for 20 min. Then, the bacteria were harvested, washed, and resuspended in PBS. Calcein-AM (5 μM) and PI (5 μM) were added to each sample and incubated in the dark for 15 min. Fluorescent images of stained bacteria were obtained by a fluorescence microscope Axio Scope A1 (Zeiss, Oberkochen, Germany).

TEM and SEM analysis

Bacterial cultures of *S. cohnii* L5, *E. faecium* E1077, *L. monocytogenes* NH1, and *E. coli* MLS9F at mid-log phase in BHI medium were collected and then resuspended in PBS to achieve a concentration of approximately 1×10^{10} CFUs/ml. *S. cohnii* L5 was treated with NCBP1 (160 μM) at 37°C for 0, 30, 60, 240, and 480 min; *E. faecium*

E1077, *L. monocytogenes* NH1, and *E. coli* MLS9F were treated with NCBP1 (512 μM) at 37°C for 480 min. Then, the bacteria were fixed in 2.5% glutaraldehyde solution, washed with 0.1 M PBS, and dehydrated with a series of ethanol concentrations (30, 50, 70, 80, 90, and 100%) for SEM analysis. For TEM analysis, the samples were embedded in Spurr epoxy resin medium and polymerized for 3 days at 70°C. Ultrathin sections were subsequently cut using an Ultracut microtome UC7 (Leica, Frankfurt, Germany) and stained with uranyl acetate and lead citrate. The scanning electron micrographs of bacterial cells were captured using a HITACHI SU-3500 SEM (Hitachi, Tokyo, Japan), and transmission electron micrographs were examined by a JEOL JEM-1400 TEM (Hitachi, Tokyo, Japan).

Membrane depolarization assay

Membrane depolarization assay was performed as described in a previous study (*67*). To simplify, *S. cohnii* L5 cultures were washed and suspended in 5 mM Hepes (pH 7, plus 5 mM glucose) to achieve an $OD_{600\ nm}$ of 0.5. Then, 1 μM $DiSC_3(5)$ (Aladdin, Shanghai, China, D131315) was added and incubated for balance at 37°C. Later, different concentrations (16, 32, and 64 μM) of NCBP1 were added and the fluorescence was measured every 10 min using an excitation wavelength of 622 nm and an emission wavelength of 670 nm with Infinite M200 Microplate reader (Tecan, Männedorf, Switzerland).

ROS measurement

The ROS measurement was conducted following the protocol outlined in a previous study (*26*). Briefly, 10 μM of 2′,7′-dichlorofluorescein diacetate (Beyotime, Shanghai, China, S0033) was added to *S. cohnii* L5 with an $OD_{600\ nm}$ of 0.5, and the samples were incubated at 37°C for 30 min. Subsequently, the samples were washed three times with 0.01 M PBS. Next, 190 μl of probe-labeled bacterial cells were mixed with 10 μl of NCBP1 at various concentrations (16, 32, and 64 μM). After incubation for 10 min, the fluorescence intensity was immediately measured using an Infinite M200 Microplate reader (Tecan, Männedorf, Switzerland) with an excitation wavelength of 488 nm and an emission wavelength of 525 nm.

ATP determination

S. cohnii L5 with an $OD_{600\ nm}$ of 0.5 in PBS was treated with varying concentrations (16, 32, and 64 μM) of NCBP1 for 10 min. The mixture was then centrifuged at 12,000*g* and 4°C for 5 min, and the resulting supernatant was collected to measure extracellular ATP levels in the model of luminescence by an Infinite M200 Microplate reader (Tecan, Männedorf, Switzerland). For intracellular ATP levels, the precipitates of *S. cohnii* L5 were lysed by lysostaphin (1 mg/ml). Then, the suspension was centrifuged and the supernatant was collected for intracellular ATP level measurement. The Enhanced ATP Assay Kit (Beyotime, Shanghai, China, S0027) was used. Before adding the test samples, the detecting solution was added to the 96-well plate for 5 min to minimize background interference (*26*).

Transcriptomic analysis

To prepare for transcriptome sequencing, *S. cohnii* L5 were cultured to exponential phase at 37°C with shaking at 200 rpm and subsequently diluted in MHB to a concentration of 10^6 to 1×10^7 CFUs/ml. After incubation with NCBP1 (at 0, 4×, and 10× MIC) for 10 min, or with NCBP1 (at 0.5× MIC) for 8 hours, bacterial cells were harvested for analysis. Total RNA was extracted from the samples using the RNAprep Pure Cell/Bacteria Kit (Tiangen, Beijing, China, DP430) and quantified via the absorbance ratio (260/280 nm) using a NanoDrop spectrophotometer (Thermo Fisher Scientific, Waltham, USA). RNA-seq was performed using Hiseq2000 (Illumina, San Diego, USA) with 150-bp paired-end reads. Raw sequencing reads were filtered by quality control and mapped against the genome of *S. cohnii* L5. Further analyses were conducted in Beijing Sinobiocore Biological Technology Co. Ltd. (Beijing, China). DEGs were identified by gene expression-level analysis using the FPKM (fragments per kilobase of transcript per million mapped reads) method with *P* values ≤0.05 and |log2 (fold change)| ≥ 1. Differences between the various treatments were analyzed using the Cuffdiff program (http://cufflinks.cbcb.umd.edu/).

qRT-PCR analysis

S. cohnii L5 was cultured to exponential phase at 37°C with shaking at 200 rpm and subsequently diluted in MHB to a concentration of 1×10^6 to 1×10^7 CFUs/ml. After incubation with NCBP1 (at 0, 4×, and 10× MIC) for 10 min, bacterial cells were harvested for analysis. Total RNA was extracted from the samples using the RNAprep Pure Cell/Bacteria Kit (Tiangen, Beijing, China, DP430) and quantified via the absorbance ratio (260/280 nm) using a NanoDrop spectrophotometer (Thermo Fisher Scientific, Waltham, USA). Reverse transcription of 1 μg of extracted RNA was performed using the Hifair III 1st Strand cDNA Synthesis SuperMix for qPCR (Yeasen, Shanghai, China, 11141) following the manufacturer's protocol. The expression levels of key genes relative to the control gene (16S ribosomal RNA) in treated *S. cohnii* L5 were determined by qRT-PCR tests with Hieff qPCR SYBR Green Master Mix (Yeasen, Shanghai, China, 11201) (*67*). The fold changes of gene expression were determined using the $2^{-\Delta\Delta Ct}$ method.

Safety assessment

The safety of NCBP1 was determined as described previously (*68*). To determine the hemolytic activity of NCBP1, fresh sterile defibrinated sheep blood cells (Yuanye, Shanghai, China, MP20026) were treated with various concentrations (ranging from 0 to 512 μM) of NCBP1 at 37°C for 1 hour, while PBS (0.01 M, pH 7.4) in the presence of 0.2% Triton X-100 was used as the control. The absorption of released hemoglobin was measured at 576 nm using an Infinite M200 Microplate reader (Tecan, Männedorf, Switzerland), and the hemolysis rate was calculated using the following formula

$$\text{Hemolysis}\ (\%) = \left[\left(OD_{576\ \text{sample}} - OD_{576\ \text{blank}}\right) / \left(OD_{576\ 0.1\%\text{Triton X}-100} - OD_{576\ \text{blank}}\right)\right] \times 100\% \quad (1)$$

To evaluate the cytotoxicity of NCBP1 on mammalian cells, Vero, HEp-2, A549, or H9c2 cells (1×10^4 cells) were mixed with various concentrations (ranging from 0 to 512 μM) of NCBP1 in 96-well plates. After incubation at 37°C for 24 hours, the cytotoxicity was assessed using the water-soluble tetrazolium salt-1 (WST-1, Roche, Basel, Switzerland, CELLPRO-RO) assay, and the absorbance was measured at 450 nm. DMEM with 10% FBS but no NCBP1 treatment was used as the negative control, and DMEM with 10% FBS but without cells was used as the blank control. The cell viability rate was calculated using the following formula

$$\text{Cell viability}\ (\%) = \left(OD_{\text{NCBP1}} - OD_{\text{blank}}\right) / \left(OD_{\text{negative control}} - OD_{\text{blank}}\right) \times 100\% \quad (2)$$

In vivo toxicity experiments

In vivo toxicity experiments were conducted to assess the safety of NCBP1, following a previously published method with slight modifications (*69*). BALB/c mice ($n = 5$ per group) were intraperitoneally injected with NCBP1 at three doses: 50, 100, and 150 mg/kg. Each concentration was tested on five mice. Throughout a 5-day monitoring period following injection, any occurrences of mortality were recorded.

Stability assessment

To evaluate the stability of NCBP1, we determined its thermostability and pH stability following the previous study (*68*). Briefly, NCBP1 was incubated at temperatures ranging from 25° to 100°C for 1 and 2 hours, or at pH levels ranging from 2 to 12 at 37°C for 1 and 2 hours, respectively. Subsequently, all samples were readjusted to pH 6.5 to measure their antibacterial activity. The residual antibacterial activity was evaluated using *S. cohnii* L5 as a model strain.

Mouse infection models

The in vivo efficacy of NCBP1 was evaluated using a murine wound infection model and a mouse peritonitis-sepsis model. For the mouse skin wound infection model, BALB/c female mice ($n = 6$ per group) were anesthetized with tribromoethanol (200 mg/kg) and their dorsal regions were shaved and disinfected with alcohol. Wounds (10 mm diameter) were created using surgical punches, and each wound was inoculated with a suspension containing 1×10^7 CFUs of *S. cohnii* L5 in PBS (0.01 M, pH 7.4). NCBP1 (8 mg/kg) or vancomycin (10 mg/kg) was dropped directly to the entire wounds 1 hour postinfection, while PBS was used as the negative control. The wound size and body weight were monitored for 10 days. Last, two representative wounds from each group were excised completely and subsequently fixed in 10% formalin for paraffin embedding, the wound skin and liver of 4 mice were excised for homogenization and bacterial burden quantification. The wound area was calculated by ImageJ (Version 1.8.0). To evaluate wound healing, histological analysis was performed using H&E (*70*) and Masson Trichrome staining techniques.

For the mouse peritonitis-sepsis model, BALB/c female mice ($n = 6$ per group) were infected with a dose of 2.0×10^9 CFUs of *S. cohnii* L5 suspension via intraperitoneal injection. At 1 hour postinfection, PBS, NCBP1 (55 and 110 mg/kg), or vancomycin (110 mg/kg) was injected intraperitoneally. Once the infected mice died, organs including the heart, liver, spleen, lung, and kidney were collected and homogenized in sterile PBS. Serial dilutions of each suspension were plated on TSA for the enumeration of bacterial colonies in different organs. At 72 hours postinfection, the surviving mice were euthanized and the bacterial colonies were calculated as mentioned above.

Antifungal activity of NCBP1 and its derivatives

NCBP1 solutions were added to the potato dextrose agar medium (PDA, Solarbio, Beijing, China, P8931) to a final concentration of 50, 75, 100, 150, and 200 μM, while its derivatives were prepared at a final concentration of 100 μM. Sterile water was used as the control. Four fungal strains (*B. maydis*, *F. verticillioides*, *C. lunata*, and *F. proliferatum*) stored at 4°C were revived on PDA plates for 4 days to obtain highly active strains and then cultured for another 4 days to complete the assay in newly prepared PDA medium. A 5-mm mycelial plug obtained from the edge of each fungal colony was placed in the center of the PDA medium containing NCBP1, derivatives, or sterile water. The plates were incubated at 28°C in the dark for 60 hours. The mycelium growth inhibition rate was determined by measuring the diameter of the fungal colony and calculated using the following equation (*71*)

$$I\,(\%) = \left[(C-d)-(T-d)\right]/(C-d)\times 100\% \quad (3)$$

where C represents the diameter of the control colony, d is the diameter of the original mycelial disk (5 mm), and T is the diameter of the colony treated with NCBP1 or its derivatives.

SCLB resistance evaluation

The *B. maydis* pathogen was prepared as previously described (*39*). Briefly, *B. maydis* was grown on PDA at 25°C for 1 week. The sterilized sorghum grains were inoculated with the fungal mat and incubated at room temperature for 4 weeks. Then, the spores were collected by flooding the surface of the sorghum grains with sterile water, and a spore suspension of 1.0×10^5 spores/ml containing 0.1% Tween-20 was prepared. Maize plants were grown in a greenhouse under a 14-hour light (28°C)/10-hour dark (25°C) photoperiod to three-leaf stage. Each plant was sprayed with 5 ml of the spore suspension, followed by treatment of the leaves ($n = 12$ per group) with either NCBP1 (50 μM) or sterile water as the control after 12 hours. Four days postinoculation, the fourth leaves were measured for the percentage of necrotic leaf area using ImageJ (Version 1.8.0). To quantify *B. maydis* DNA content, qRT-PCR was performed using specific primers targeting the *ITS* gene of *B. maydis* (BMF-3 and BMR-3, table S8). Maize DNA was quantified using primers specific to the *Ef1a* gene (Ef1a-F and Ef1a-R, table S8).

Cellular analysis of maize plants infected with *B. Maydis*

To assess the morphological changes caused by *B. maydis* infection (*72*), 1-μm sections of leaf tissue were obtained from the same position, 10 cm from the leaf tip, in both NCBP1-treated and control plants using a Leica RM2016 ultramicrotome (Leica, Frankfurt, Germany). Then, the sections were stained using periodic acid–Schiff reagents (Pinuofei, Wuhan, China, P0046). All samples were observed using the Digital Pathology Slide Scanner KF-FL-400 (Jiangfeng, Yuyao, China).

Seed rot resistance evaluation

The evaluation of seed rot resistance was conducted as described previously (*73*). *F. verticillioides* cultured on PDA medium was transferred to maize seed media and incubated at 28°C in the dark for 7 to 10 days. Conidia were harvested and suspended in sterile water (1×10^5 spores/ml). Twenty B73 maize seeds with uniform size and quality were surface sterilized and then incubated with *F. verticillioides* in the dark for 24 hours. After incubation, seeds were treated with NCBP1 (50 μM) for an additional 24 hours. The necrotic seed area was measured using ImageJ (Version 1.8.0). The expression level of *F. verticillioides Tubulin* gene (Tubulin-F and Tubulin-R, table S8) determined by qRT-PCR was used to quantify *F. verticillioides* content. Maize *Ef1a* gene (Ef1a-F and Ef1a-R, table S8) was used as the internal control. In addition, the fumonisin levels in maize seeds were determined using Immunoaffinity Column Purification-Precolumn Derivatization High-Performance Liquid Chromatography (LC-20A) (Shimadzu Corporation, Kyoto, Japan),

in accordance with the National Standard of the People's Republic of China GB5009.240-2023.

Bioinformatics analysis

GSEA was displayed using the local version of the GSEA analysis tool (http://broadinstitute.org/gsea/index.jsp). Volcano plots were performed using R software (Version 3.5.1). PCA and heatmap plots were conducted using the OmicShare tools, a free online platform for data analysis (https://www.omicshare.com/tools/).

Statistical analysis

Statistical analysis was performed using GraphPad Prism V.8.0.2. Data were presented as means ± SD, based on at least three independent biological samples. $P < 0.05$ was considered statistically significant.

Supplementary Materials

The PDF file includes:

Figs. S1 to S13
Legends for tables S1, S2, and S7
Tables S3 to S6 and S8
Legends for data S1 and S2

Other Supplementary Material for this manuscript includes the following:

Tables S1, S2, and S7
Data S1 and S2

REFERENCES AND NOTES

1. B. Gollan, G. Grabe, C. Michaux, S. Helaine, Bacterial persisters and infection: Past, present, and progressing. *Annu. Rev. Microbiol.* **73**, 359–385 (2019).
2. K. Lewis, The science of antibiotic discovery. *Cell* **181**, 29–45 (2020).
3. C. L. Ventola, The antibiotic resistance crisis: Part 1: Causes and threats. *P. T.* **40**, 277–283 (2015).
4. R. Laxminarayan, D. Sridhar, M. Blaser, M. G. Wang, M. Woolhouse, Achieving global targets for antimicrobial resistance. *Science* **353**, 874–875 (2016).
5. H. F. Chambers, F. R. Deleo, Waves of resistance: *Staphylococcus aureus* in the antibiotic era. *Nat. Rev. Microbiol.* **7**, 629–641 (2009).
6. C. Willyard, The drug-resistant bacteria that pose the greatest health threats. *Nature* **543**, 15 (2017).
7. Y. X. Ma, C. Y. Wang, Y. Y. Li, J. Li, Q. Q. Wan, J. H. Chen, F. R. Tay, L. N. Niu, Considerations and caveats in combating ESKAPE pathogens against nosocomial infections. *Adv. Sci.* **7**, 1901872 (2020).
8. P. Tavormina, B. D. Coninck, N. Nikonorova, I. D. Smet, B. P. A. Cammue, The plant peptidome: An expanding repertoire of structural features and biological functions. *Plant Cell.* **27**, 2095–2118 (2015).
9. M. Zasloff, Antimicrobial peptides of multicellular organisms. *Nature* **415**, 389–395 (2002).
10. R. E. W. Hancock, H. G. Sahl, Antimicrobial and host-defense peptides as new anti-infective therapeutic strategies. *Nat. Biotechnol.* **24**, 1551–1557 (2006).
11. M. Xiong, M. W. Lee, R. A. Mansbach, Z. Song, Y. Bao, R. M. Peek, C. Yao, L. F. Chen, A. L. Ferguson, G. C. L. Wong, Helical antimicrobial polypeptides with radial amphiphilicity. *Proc. Natl. Acad. Sci. U.S.A.* **112**, 13155–13160 (2015).
12. W. F. Porto, L. Irazazabal, E. S. F. Alves, S. M. Ribeiro, C. O. Matos, Á. S. Pires, I. C. M. Fensterseifer, V. J. Miranda, E. F. Haney, V. Humblot, M. D. T. Torres, R. E. W. Hancock, L. M. Liao, A. Ladram, T. K. Lu, C. de la Fuente-Nunez, O. L. Franco, In silico optimization of a guava antimicrobial peptide enables combinatorial exploration for peptide design. *Nat. Commun.* **9**, 1490 (2018).
13. C. M. de Souza, Á. P. da Silva, N. G. O. Júnior, O. F. Martínez, O. L. Franco, Peptides as a therapeutic strategy against *Klebsiella pneumoniae*. *Trends Pharmacol. Sci.* **43**, 335–348 (2022).
14. J. Xuan, W. Feng, J. Wang, R. Wang, B. Zhang, L. Bo, Z. S. Chen, H. Yang, L. Sun, Antimicrobial peptides for combating drug-resistant bacterial infections. *Drug Resist. Updat.* **68**, 100954 (2023).
15. D. I. Andersson, D. Hughes, J. Z. Kubicek-Sutherland, Mechanisms and consequences of bacterial resistance to antimicrobial peptides. *Drug Resist. Updat.* **26**, 43–57 (2016).
16. G. H. Gudmundsson, B. Agerberth, J. Odeberg, T. Bergman, B. Olsson, R. Salcedo, The human gene *FALL39* and processing of the cathelin precursor to the antibacterial peptide LL-37 in granulocytes. *Eur. J. Biochem.* **238**, 325–332 (1996).
17. Y. Liu, S. Ding, J. Shen, K. Zhu, Nonribosomal antibacterial peptides that target multidrug-resistant bacteria. *Nat. Prod. Rep.* **36**, 573–592 (2019).
18. S. Biswas, J. M. Brunel, J. C. Dubus, M. Reynaud-Gaubert, J. M. Rolain, Colistin: An update on the antibiotic of the 21st century. *Expert Rev. Anti Infect. Ther.* **10**, 917–934 (2012).
19. A. Peschel, H. G. Sahl, The co-evolution of host cationic antimicrobial peptides and microbial resistance. *Nat. Rev. Microbiol.* **4**, 529–536 (2006).
20. Y. Hu, F. Liu, I. Y. C. Lin, G. F. Gao, B. Zhu, Dissemination of the *mcr-1* colistin resistance gene. *Lancet Infect. Dis.* **16**, 146–147 (2016).
21. J. Li, D. Liu, X. Tian, S. Koseki, S. Chen, X. Ye, T. Ding, Novel antibacterial modalities against methicillin resistant *Staphylococcus aureus* derived from plants. *Crit. Rev. Food Sci. Nutr.* **59**, S153–S161 (2019).
22. S. Wang, L. Tian, H. Liu, X. Li, J. Zhang, X. Chen, X. Jia, X. Zheng, S. Wu, Y. Chen, J. Yan, L. Wu, Large-scale discovery of non-conventional peptides in maize and *Arabidopsis* through an integrated peptidogenomic pipeline. *Mol. Plant* **13**, 1078–1093 (2020).
23. S. Plaza, G. Menschaert, F. Payre, In search of lost small peptides. *Annu. Rev. Cell Dev. Biol.* **33**, 391–416 (2017).
24. J. Chen, A. D. Brunner, J. Z. Cogan, J. K. Nuñez, A. P. Fields, B. Adamson, D. N. Itzhak, J. Y. Li, M. Mann, M. D. Leonetti, J. S. Weissman, Pervasive functional translation of noncanonical human open reading frames. *Science* **367**, 1140–1146 (2020).
25. R. Jackson, L. Kroehling, A. Khitun, W. Bailis, A. Jarret, A. G. York, O. M. Khan, J. R. Brewer, M. H. Skadow, C. Duizer, C. C. D. Harman, L. Chang, P. Bielecki, A. G. Solis, H. R. Steach, S. Slavoff, R. A. Flavell, The translation of non-canonical open reading frames controls mucosal immunity. *Nature* **564**, 434–438 (2018).
26. M. Song, Y. Liu, T. Li, X. Liu, Z. Hao, S. Ding, P. Panichayupakaranant, K. Zhu, J. Shen, Plant natural flavonoids against multidrug resistant pathogens. *Adv. Sci.* **8**, e2100749 (2021).
27. W. Wang, W. Li, Z. Wen, C. Wang, W. Liu, Y. Zhang, J. Liu, T. Ding, L. Shuai, G. Zhong, Z. Bu, L. Qu, M. Ren, F. Li, Gossypol broadly inhibits coronaviruses by targeting RNA-dependent RNA polymerases. *Adv. Sci.* **9**, e2203499 (2022).
28. M. Moller, E. H. Stukenbrock, Evolution and genome architecture in fungal plant pathogens. *Nat. Rev. Microbiol.* **15**, 771 (2017).
29. C. Imjongjirak, P. Amparyup, A. Tassanakajon, Two novel antimicrobial peptides, arasin-likeSp and GRPSp, from the mud crab *Scylla paramamosain*, exhibit the activity against some crustacean pathogenic bacteria. *Fish Shellfish Immunol.* **30**, 706–712 (2011).
30. S. Leroy, A. Vermassen, R. Talon, *Staphylococcus*: Occurrence and properties, in *Encyclopedia of Food and Health*, B. Caballero, P. M. Finglas, F. Toldrá, Eds. (Elsevier, 2016), vol. 5, pp. 140–145.
31. D. Roccatano, G. Colombo, M. Fioroni, A. E. Mark, Mechanism by which 2,2,2-trifluoroethanol/water mixtures stabilize secondary-structure formation in peptides: A molecular dynamics study. *Proc. Natl. Acad. Sci. U.S.A.* **99**, 12179–12184 (2002).
32. Z. Wang, D. Teng, R. Mao, Y. Hao, N. Yang, X. Wang, J. Wang, A cleavable chimeric peptide with targeting and killing domains enhances LPS neutralization and antibacterial properties against multi-drug resistant *E. coli*. *Commun. Biol.* **6**, 1170 (2023).
33. K. P. Adamala, A. E. Engelhart, J. W. Szostak, Collaboration between primitive cell membranes and soluble catalysts. *Nat. Commun.* **7**, 11041 (2016).
34. S. Lohan, D. Mandal, W. Choi, A. G. Konshina, R. K. Tiwari, R. G. Efremov, I. Maslennikov, K. Parang, Small amphiphilic peptides: Activity against a broad range of drug-resistant bacteria and structural insight into membranolytic properties. *J. Med. Chem.* **65**, 665–687 (2022).
35. H. Tang, Y. Liu, B. Li, B. Shang, J. Yang, C. Zhang, L. Yang, K. Chen, W. Wang, J. Liu, Water-soluble PANI:PSS designed for spontaneous non-disruptive membrane penetration and direct intracellular photothermal damage on bacteria. *Bioact. Mater.* **6**, 4758–4771 (2021).
36. D. Albanesi, G. Reh, M. E. Guerin, F. Schaeffer, M. Debarbouille, A. Buschiazzo, G. E. Schujman, D. de Mendoza, P. M. Alzari, Structural basis for feed-forward transcriptional regulation of membrane lipid homeostasis in *Staphylococcus aureus*. *PLOS Pathog.* **9**, e1003108 (2013).
37. J. I. Yeh, U. Chinte, S. Du, Structure of glycerol-3-phosphate dehydrogenase, an essential monotopic membrane enzyme involved in respiration and metabolism. *Proc. Natl. Acad. Sci. U.S.A.* **105**, 3280–3285 (2008).
38. E. Stukenbrock, S. Gurr, Address the growing urgency of fungal disease in crops. *Nature* **617**, 31–34 (2023).
39. C. Chen, Y. Zhao, G. Tabor, H. Nian, J. Phillips, P. Wolters, Q. Yang, P. Balint-Kurti, A leucine-rich repeat receptor kinase gene confers quantitative susceptibility to maize southern leaf blight. *New Phytol.* **238**, 1182–1197 (2023).
40. P. Ma, E. Liu, Z. Zhang, T. Li, Z. Zhou, W. Yao, J. Chen, J. Wu, Y. Xu, H. Zhang, Genetic variation in *ZmWAX2* confers maize resistance to *Fusarium verticillioides*. *Plant Biotechnol. J.* **21**, 1812–1826 (2023).
41. E. G. Magny, J. I. Pueyo, F. M. G. Pearl, M. A. Cespedes, J. E. Niven, S. A. Bishop, J. P. Couso, Conserved regulation of cardiac calcium uptake by peptides encoded in small open reading frames. *Science* **341**, 1116–1120 (2013).
42. T. Kondo, S. Plaza, J. Zanet, E. Benrabah, P. Valenti, Y. Hashimoto, S. Kobayashi, F. Payre, Y. Kageyama, Small peptides switch the transcriptional activity of Shavenbaby during *Drosophila* embryogenesis. *Science* **329**, 336–339 (2010).

43. B. R. Nelson, C. A. Makarewich, D. M. Anderson, B. R. Winders, C. D. Troupes, F. Wu, A. L. Reese, J. R. Mcanally, X. Chen, E. T. Kavalali, A peptide encoded by a transcript annotated as long noncoding RNA enhances SERCA activity in muscle. *Science* **351**, 271–275 (2016).
44. A. Matsumoto, A. Pasut, M. Matsumoto, R. Yamashita, J. Fung, E. Monteleone, A. Saghatelian, K. I. Nakayama, J. G. Clohessy, P. P. Pandolfi, mTORC1 and muscle regeneration are regulated by the LINC00961-encoded SPAR polypeptide. *Nature* **541**, 228–232 (2017).
45. A. G. Hinnebusch, I. P. Ivanov, N. Sonenberg, Translational control by 5′-untranslated regions of eukaryotic mRNAs. *Science* **352**, 1413–1416 (2016).
46. J. P. Couso, P. Patraquim, Classification and function of small open reading frames. *Nat. Rev. Mol. Cell Biol.* **18**, 575–589 (2017).
47. C. M. Laumont, T. Daouda, J. P. Laverdure, E. Bonneil, O. Caron-Lizotte, M. P. Hardy, D. P. Granados, C. Durette, S. Lemieux, P. Thibault, C. Perreault, Global proteogenomic analysis of human MHC class I-associated peptides derived from non-canonical reading frames. *Nat. Commun.* **7**, 10238 (2016).
48. D. Lauressergues, J. M. Couzigou, H. S. Clemente, Y. Martinez, C. Dunand, G. Becard, J. P. Combier, Primary transcripts of microRNAs encode regulatory peptides. *Nature* **520**, 90–93 (2015).
49. A. Sharma, P. K. Badola, C. Bhatia, D. Sharma, P. K. Trivedi, Primary transcript of miR858 encodes regulatory peptide and controls flavonoid biosynthesis and development in *Arabidopsis*. *Nat. Plants.* **6**, 1262–1274 (2020).
50. P. K. Badola, A. Sharma, H. Gautam, P. K. Trivedi, MicroRNA858a, its encoded peptide, and phytosulfokine regulate Arabidopsis growth and development. *Plant Physiol.* **189**, 1397–1415 (2022).
51. M. F. Burton, P. G. Steel, The chemistry and biology of LL-37. *Nat. Prod. Rep.* **26**, 1572–1584 (2009).
52. J. Sun, H. Zhang, Y. H. Liu, Y. Feng, Towards understanding MCR-like colistin resistance. *Trends Microbiol.* **26**, 794–808 (2018).
53. J. P. Tam, S. Wang, K. H. Wong, W. L. Tan, Antimicrobial peptides from plants. *Pharmaceuticals* **8**, 711–757 (2015).
54. J. Lin, D. Zhou, T. A. Steitz, Y. S. Polikanov, M. G. Gagnon, Ribosome-targeting antibiotics: Modes of action, mechanisms of resistance, and implications for drug design. *Annu. Rev. Biochem.* **87**, 451–478 (2018).
55. N. Vazquez-Laslop, A. S. Mankin, How macrolide antibiotics work. *Trends Biochem. Sci.* **43**, 668–684 (2018).
56. C. Sohlenkamp, O. Geiger, Bacterial membrane lipids: Diversity in structures and pathways. *FEMS Microbiol. Rev.* **40**, 133–159 (2016).
57. K. Wang, W. Dang, J. Xie, R. Zhu, M. Sun, F. Jia, Y. Zhao, X. An, S. Qiu, X. Li, Z. Ma, W. Yan, R. Wang, Antimicrobial peptide protonectin disturbs the membrane integrity and induces ROS production in yeast cells. *Biochim. Biophys. Acta Biomembr.* **1848**, 2365–2373 (2015).
58. E. Holaskova, P. Galuszka, I. Frebort, M. T. Oz, Antimicrobial peptide production and plant-based expression systems for medical and agricultural biotechnology. *Biotechnol. Adv.* **33**, 1005–1023 (2015).
59. Y. Fu, B. Xie, D. Ben, K. Lv, S. Zhu, W. Lu, H. Tang, D. Cheng, B. Ma, G. Wang, S. Xiao, G. Wang, Z. Xia, Pathogenic alteration in severe burn wounds. *Burns* **38**, 90–94 (2012).
60. E. Montesinos, Functional peptides for plant disease control. *Annu. Rev. Phytopathol.* **61**, 301–324 (2023).
61. F. N. Kushanov, O. S. Turaev, O. A. Muhammadiyev, R. F. Umarov, N. M. Rakhimova, N. N. Mamadaliyeva, Maize (*Zea mays* L.) as a model system for plant genetic, genomic, and applied research, in *Model Organisms in Plant Genetics*, I. Y. Abdurakhmonov, Ed. (IntechOpen, 2022).
62. E. Jurrus, D. Engel, K. Star, K. Monson, J. Brandi, L. E. Felberg, D. H. Brookes, L. Wilson, J. Chen, K. Liles, M. Chun, P. Li, D. W. Gohara, T. Dolinsky, R. Konecny, D. R. Koes, J. E. Nielsen, T. Head-Gordon, W. Geng, R. Krasny, G. W. Wei, M. J. Holst, J. A. McCammon, N. A. Baker, Improvements to the APBS biomolecular solvation software suite. *Protein Sci.* **27**, 112–128 (2018).
63. M. M. M. Goudet, D. J. Orr, M. Melkonian, K. H. Muller, M. T. Meyer, E. Carmo-Silva, H. Griffiths, Rubisco and carbon-concentrating mechanism co-evolution across chlorophyte and streptophyte green algae. *New Phytol.* **227**, 810–823 (2020).
64. S. Daly, F. Rosu, V. Gabelica, Mass-resolved electronic circular dichroism ion spectroscopy. *Science* **368**, 1465–1468 (2020).
65. C. J. Wienken, P. Baaske, U. Rothbauer, D. Braun, S. Duhr, Protein-binding assays in biological liquids using microscale thermophoresis. *Nat. Commun.* **1**, 100 (2010).
66. M. A. Tomeh, R. Hadianamrei, W. Sun, D. Xu, S. Brown, X. Zhao, Stiffness-tuneable nanocarriers for controlled delivery of ASC-J9 into colorectal cancer cells. *J. Colloid Interface Sci.* **594**, 513–521 (2021).
67. M. Song, Y. Liu, X. Huang, S. Ding, Y. Wang, J. Shen, K. Zhu, A broad-spectrum antibiotic adjuvant reverses multidrug-resistant Gram-negative pathogens. *Nat. Microbiol.* **5**, 1040–1050 (2020).
68. Y. Liu, S. Ding, R. Dietrich, E. Martlbauer, K. Zhu, A biosurfactant-inspired heptapeptide with improved specificity to kill MRSA. *Angew. Chem. Int. Ed.* **56**, 1486–1490 (2017).
69. J. L. Narayana, B. Mishra, T. Lushnikova, Q. Wu, Y. S. Chhonker, Y. Zhang, D. Zarena, E. S. Salnikov, X. Dang, F. Wang, C. Murphy, K. W. Foster, S. Gorantla, B. Bechinger, D. J. Murry, G. Wang, Two distinct amphipathic peptide antibiotics with systemic efficacy. *Proc. Natl. Acad. Sci. U.S.A.* **117**, 19446–19454 (2020).
70. A. H. Fischer, K. A. Jacobson, J. Rose, R. Zeller, Hematoxylin and eosin staining of tissue and cell sections. *Cold Spring Harb. Protoc.* **5**, pdb.prot4986 (2008).
71. L. Tian, X. Chen, X. Jia, S. Wang, X. Wang, J. Zhang, Y. Zhang, S. Wu, Y. Chen, L. Wu, First report of antifungal activity conferred by non-conventional peptides. *Plant Biotechnol. J.* **19**, 2147–2149 (2021).
72. J. Zhang, X. Jia, G. F. Wang, S. Ma, S. Wang, Q. Yang, X. Chen, Y. Zhang, Y. Lyu, X. Wang, J. Shi, Y. Zhao, Y. Chen, L. Wu, Ascorbate peroxidase 1 confers resistance to southern corn leaf blight in maize. *J. Integr. Plant Biol.* **64**, 1196–1211 (2022).
73. P. Ma, H. Li, E. Liu, K. He, Y. Song, C. Dong, Z. Wang, X. Zhang, Z. Zhou, Y. Xu, J. Wu, H. Zhang, Evaluation and identification of resistance lines and QTLs of maize to seedborne *Fusarium verticillioides*. *Plant Dis.* **106**, 2066–2073 (2022).

Acknowledgments: We thank S.-B. Wu (University of New England, Australia) for constructive comments and suggestions on the manuscript. **Funding:** This study was supported by the funding sources listed as follows: National Key Research and Development Program of China grants 2022YFD1201802 (L.W.) and 2022YFD1801600 (K.Z.) and National Natural Science Foundation of China grants 32172073 (L.W.), U22A20474 (L.W.), and U23A20241 (X.-D.D.). **Author contributions:** Conceptualization: L.W., K.Z., X.C., M.S., L.T., A.S., and U.A. Methodology: X.C., M.S., X.S., J. Zhao, M.C., J.Zhan., L.W., and X.-D.D. Software: X.C., M.S., L.T., X.S., H.Y., and U.A. Validation: X.C., M.S., J. Zhao, H.Y., L.W., K.Z., and X.-D.D. Formal analysis: X.C., M.S., C.M., A.S., H.Y., L.W., K.Z., and X.-D.D. Investigation: X.C., M.S., L.T., X.S., C.M., M.C., J. Zhao, J.S., H.L., Y.Z., J.Zhan., S.W., L.W., and X.-D.D. Resources: X.C., X.S., C.M., J. Zhao, H.Y., H.L., L.W., K.Z., and X.-D.D. Data curation: X.C., M.S., A.S., H.Y., Y.C., L.W., and X.-D.D. Writing—original draft: X.C., M.S., L.T., and L.W. Writing—review and editing: X.C., M.S., L.T., A.S., U.A., S.W., C.-L.S., L.W., K.Z., and X.-D.D. Visualization: X.C., L.T., U.A., S.W., Y.C., and L.W. Supervision: L.W., K.Z., and X.-D.D. Project administration: L.W., K.Z., and X.-D.D. Funding acquisition: L.W. and K.Z. **Competing interests:** The authors declare that they have no competing interests. **Data and materials availability:** All data needed to evaluate the conclusions in the paper are present in the paper and/or the Supplementary Materials. RNA-seq data have been deposited in the National Center for Biotechnology Information's Sequence Read Archive (NCBI SRA) under accession number PRJNA934751. Source data are provided in data S2.

Submitted 12 October 2024
Accepted 11 February 2025
Published 19 March 2025
10.1126/sciadv.adt8239